

Sensory experience regulates cortical inhibition by inducing IGF1 in VIP neurons

A. R. Mardinly^{1*}, I. Spiegel^{2*}, A. Patrizi³, E. Centofante³, J. E. Bazinet², C. P. Tzeng², C. Mandel-Brehm², D. A. Harmin², H. Adesnik¹, M. Fagiolini³ & M. E. Greenberg²

Inhibitory neurons regulate the adaptation of neural circuits to sensory experience¹, but the molecular mechanisms by which experience controls the connectivity between different types of inhibitory neuron^{2,3} to regulate cortical plasticity are largely unknown. Here we show that exposure of dark-housed mice to light induces a gene program in cortical vasoactive intestinal peptide (VIP)-expressing neurons that is markedly distinct from that induced in excitatory neurons and other subtypes of inhibitory neuron. We identify *Igf1* as one of several activity-regulated genes that are specific to VIP neurons, and demonstrate that IGF1 functions cell-autonomously in VIP neurons to increase inhibitory synaptic input onto these neurons. Our findings further suggest that in cortical VIP neurons, experience-dependent gene transcription regulates visual acuity by activating the expression of IGF1, thus promoting the inhibition of disinhibitory neurons^{3–5} and affecting inhibition onto cortical pyramidal neurons.

To explore how sensory experience affects gene expression in VIP neurons, we examined this process in the visual cortex of adult mice that were housed in standard conditions, in complete darkness (that is, dark-housed), or dark-housed and then exposed to light for increasing amounts of time^{6,7} (Fig. 1a). Light deprivation for as little as 12 h drives robust gene expression after light exposure, and increasing durations of dark-housing accentuate the gene induction response (Extended Data Fig. 1a) irrespective of the phase of the circadian rhythm (Extended Data Fig. 1b). To purify RNA selectively from VIP-expressing and other inhibitory neuron subtypes, we generated mice that were heterozygous for alleles of either *Vip-cre*, *Sst-cre* or *Pv-cre*, and were also heterozygous for the *Rpl22-HA* (RiboTag) allele⁸, which expresses a haemagglutinin (HA)-tagged ribosomal protein specifically in Cre-expressing neurons (Fig. 1a). For purposes of comparison, we also purified ribosome-bound RNA from excitatory and inhibitory neurons, labelled by *Emx1-cre* or *Gad2-cre*.

By quantitative real-time PCR (qPCR), we find that messenger RNAs for cell-type-specific marker genes are highly enriched in the appropriate samples (Extended Data Fig. 1c) and that light exposure induces the expression of early-response genes in each Cre line (Extended Data Fig. 1d). To quantify experience-induced gene expression at a genome-wide level, we performed RNA-seq on RNA isolated from the dark-housed/light-exposed RiboTag-mice (Supplementary Table 1) (Fig. 1b, c and Extended Data Fig. 2a, b). This analysis identified genes which exhibited reproducible changes in expression levels in response to visual stimulation in at least one Cre line ($n = 602$; see Supplementary Table 2 and Methods) and thus allowed us to ask how levels of these experience-regulated genes are correlated across the different neuronal subtypes compared to non-regulated genes ($n = 13,678$) (Fig. 1d–i). We found that the expression of experience-regulated genes is remarkably dissimilar across different neuronal subtypes when compared to genes that are not regulated by sensory experience (irrespective of differences in

the number or expression levels of experience-regulated genes; Fig. 1f–i and Extended Data Fig. 3a–d). While unique subsets of experience-responsive genes were identified in each neuronal subtype (Fig. 2a, b and Extended Data Fig. 3e, f), VIP neurons are the most responsive to sensory stimulation (Fig. 1d, e) and possess an experience-induced gene expression program that is markedly distinct from the other neuronal subtypes analysed (Fig. 1h, i). This suggests that in VIP neurons the experience-dependent gene program may have a unique function in adapting the cortex's neural circuits to sensory experience.

We hypothesized that experience-regulated genes that are specifically expressed and selectively regulated in VIP neurons are likely to have important functions in regulating the synaptic connectivity onto VIP neurons. Thus, we first identified the mRNAs that are specifically enriched in each subtype (Extended Data Fig. 4a; Methods) and cross-referenced these genes with the list of experience-regulated genes (Extended Data Fig. 4b). This analysis identified 31 genes that are both cell-type-specific and experience-regulated, 11 of which are specific to VIP neurons (Supplementary Table 4). Notably, secreted molecules are significantly over-represented in this gene set (GO-term 'Secreted' $P = 0.002$) and each type of neuron has its own set of cell-type-specific experience-regulated secreted factors, including four experience-induced secreted molecules that are specific to VIP neurons (*Igf1*, *Crh*, *Prok2*, *Fbln2*; Fig. 2b, Supplementary Table 4).

We next performed fluorescent *in situ* hybridization (FISH) on sections of visual cortices of dark-housed/light-exposed mice to quantify the percentage of cells that co-express an inhibitory subtype marker and the respective secreted factor (Fig. 2c–f). Of the four secreted factors, *Igf1* is the one factor that is expressed in the vast majority of VIP neurons, and whose expression is highly enriched in these neurons (Fig. 2d). We were unable to reliably identify *Fbln2*-expressing cells, and *Prok2* was expressed nearly exclusively in a sparse subpopulation of VIP neurons (Fig. 2f), consistent with the low expression level of these genes in the RiboTag-seq experiments (Extended Data Fig. 4c). While the FISH analysis revealed that in the cortex *Crh* is highly enriched in VIP neurons compared to PV and SST neurons (Fig. 2e), this gene is also expressed in *Pv-/Sst-/Vip*-negative cortical interneurons⁹. Since IGF1 is the sole experience-induced secreted factor that is selectively expressed in most VIP neurons, we focused our subsequent analysis on IGF1.

Previous reports have suggested that IGF1 is synthesized in the cortex¹⁰, but the function of cortical-derived IGF1 was unknown. Global disruption of the *Igf1* gene results in abnormally small animals with smaller brains that contain smaller neurons with dendrites that are less branched and contain fewer synapses^{11–13}, and the effects of IGF1 on brain development and function are due at least in part to IGF1 that is produced by non-neural tissues and then enters the brain¹⁴. To investigate specifically VIP neuron-derived IGF1, we crossed *Vip-cre* mice to both IGF1 conditional-knockout mice¹⁵ and Cre reporter mice. Disruption of *Igf1* specifically in VIP neurons had no effect on the

¹Department of Molecular and Cellular Biology, University of California Berkeley, 205 Life Sciences Addition, Berkeley, California 94720, USA. ²Department of Neurobiology, Harvard Medical School, 220 Longwood Ave, Boston, Massachusetts 02115, USA. ³FM Kirby Neurobiology Center, Boston Children's Hospital, 3 Blackfan Circle, Boston, Massachusetts 02115, USA.

*These authors contributed equally to this work.

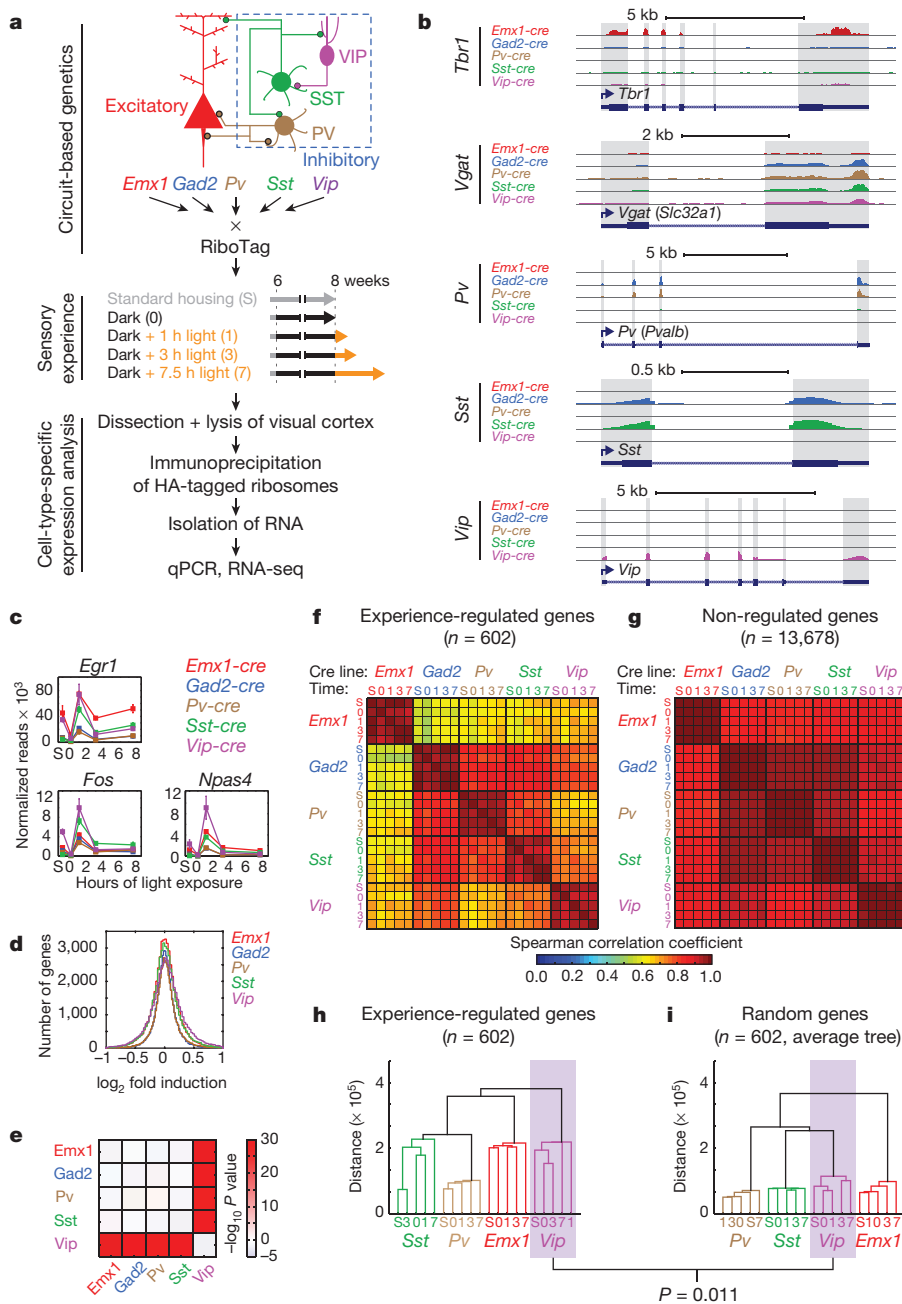


Figure 1 | VIP neurons mount a unique transcriptional response to sensory experience. **a**, Approach for purifying ribosome-bound RNA from Cre-expressing neurons in visual cortex following manipulation of visual experience. **b**, Representative RNA-seq tracks of cell-type-specific marker genes (exons shaded). **c**, Line plots showing the expression levels of selected early induced genes in each Cre line at each time point ($n = 3$, error bars, s.e.m.). **d**, Histograms showing the distribution of all observed fold-changes for each Cre line (mean of three replicates). **e**, Colour-coded matrix showing the $-\log_{10}$ P value of pairwise corrected two-tailed *t*-tests of the fold-change distributions between each Cre line. **f**, **g**, Matrices of Spearman correlation coefficients computed from the expression levels of experience-regulated genes (**f**) or genes not regulated by experience (**g**) (mean of three replicates). **h**, **i**, Cladograms of all experience-regulated genes created by using the mean values of each gene in each sample (**h**) or the average cladogram created from 1,000 random sets of 602 random genes using the mean expression values of each gene in each sample (**i**) ($P = 0.011$, Monte Carlo test).

thickness of the cortical layers, on the number and layer distribution of VIP neurons, or on the size of VIP neuron cell bodies at postnatal day 21 (that is, P21) (Extended Data Fig. 5a–d). To test whether VIP neuron-derived IGF1 affects excitatory and/or inhibitory inputs to VIP neurons, we recorded miniature inhibitory or excitatory postsynaptic currents (mIPSCs or mEPSCs) in VIP neurons in acute visual cortex slices; we found that conditional deletion of *Igf1* in VIP neurons leads to a significant reduction in mIPSC frequency (Fig. 3a) but not amplitude (Fig. 3b). Since conditional deletion of *Igf1* had no effect on the frequency or amplitude of excitatory mEPSCs on VIP neurons (Fig. 3c, d), these findings suggest that VIP-neuron-derived IGF1 specifically enhances inhibitory synaptic input onto VIP neurons.

To test whether IGF1 functions cell-autonomously to regulate inhibitory input onto the cell from which it is expressed, we used a virus-based approach to acutely knockdown *Igf1* expression in only a few VIP neurons. We generated short hairpin RNA (shRNA) constructs against *Igf1* (Extended Data Fig. 6a, b), injected low titre AAVs expressing the shRNA and Cre-dependent enhanced green fluorescent

protein (eGFP) into the visual cortex of P14–15 *Vip-cre* mice, and recorded mIPSCs and mEPSCs one week later (P20–P22) in eGFP-positive VIP neurons that are surrounded by non-infected VIP neurons (Fig. 3e). This sparse and acute knockdown of *Igf1* in VIP neurons using either of two distinct shRNAs against *Igf1* resulted in a marked reduction in mIPSC frequency and amplitude as compared to VIP neurons infected with a control shRNA (Fig. 3f, g), but had no significant effect on mEPSCs (Fig. 3h, i). These effects are not due to altered VIP neuron morphology (Fig. 3j and Extended Data Fig. 6c), indicating that VIP-neuron-derived IGF1 acutely promotes inhibition onto VIP neurons in a cell-autonomous manner.

To determine if VIP-neuron-derived IGF1 regulates inhibitory inputs onto other types of cortical neurons, we adopted a protocol that leads to widespread infection of neurons in the cortex (see Methods). Injecting AAVs into *Vip-*, *Pv-* or *Sst-cre* mice to label these cells with eGFP while knocking down *Igf1* in VIP neurons, we recorded mIPSCs from each cell type and found that early knockdown of *Igf1* in the cortex decreases mIPSCs frequency in VIP neurons, but does not affect mIPSCs onto

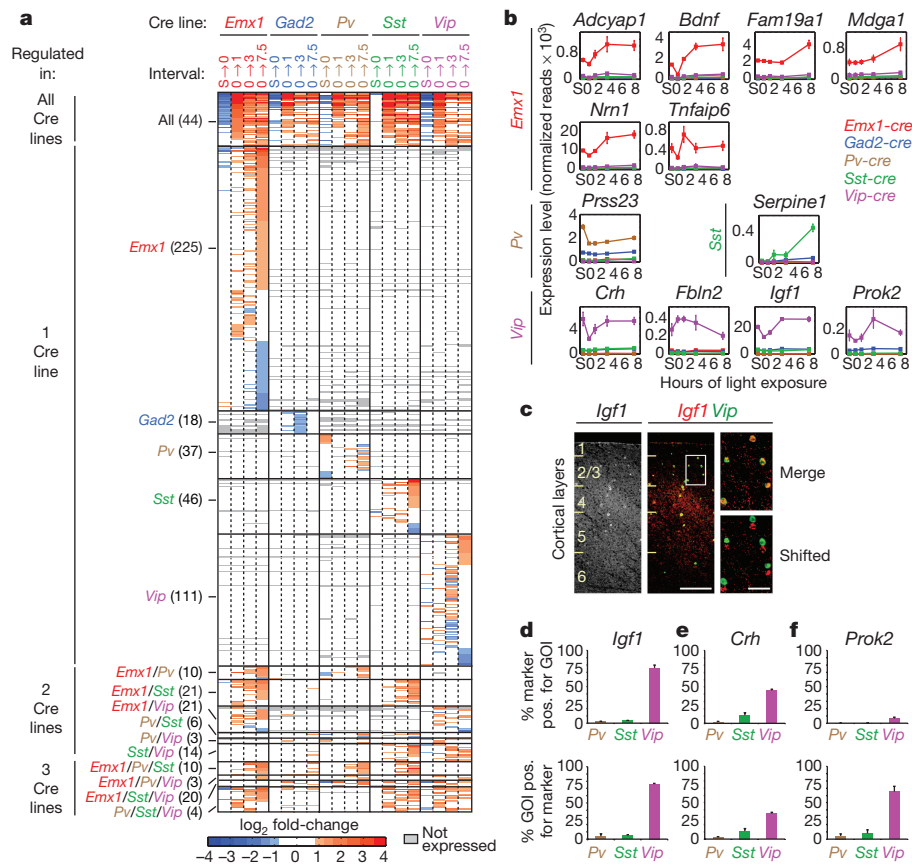


Figure 2 | IGF1 is an experience-induced cell-type-specific secreted factor in VIP neurons. **a**, Heat map showing the fold-change in expression of all experience-regulated genes across all stimulus intervals. **b**, Line plots of secreted factors that are experience-regulated and expressed in a cell-type-specific manner (n = 3, error bars, s.e.m.). **c**, Fluorescent *in situ* hybridization for *Igf1* and *Vip* in mouse visual cortex after dark housing and light exposure for 7.5 h (white box indicates the magnified area; scale bar, 200 μm in main image; 50 μm in magnification). **d-f**, Quantification of fluorescent *in situ* hybridization for *Igf1* (**d**), *Crh* (**e**), *Prok2* (**f**) and inhibitory markers in visual cortices of dark-housed/light-exposed mice (n = 3, bars represent s.e.m.). GOI, gene of interest.

PV, SST, or pyramidal neurons (Extended Data Fig. 6e–l). Furthermore, ELISA-based analysis of IGF1 levels in the blood of mice whose cortices were injected with these viruses demonstrated that removing IGF1 from VIP neurons did not alter the level of serum-derived IGF1 (Extended Data Fig. 6d). While we formally cannot exclude that serum-derived IGF1 contributes to inhibition onto VIP neurons, this finding indicates that the decrease in mIPSCs in VIP neurons that express *Igf1* shRNAs is due at least in part to reduced *Igf1* expression in VIP neurons. Thus, VIP-neuron-derived IGF1 regulates the inhibitory inputs onto the VIP neuron in which it is produced, probably via local release from VIP neurons. Consistent with this idea, we find that the *Igf1* splice variant expressed by VIP neurons encodes an isoform of IGF1 containing a heparin binding domain (*Igf1.4*; Extended Data Fig. 7a) that may limit the diffusion of IGF1 and facilitate its local action¹⁶.

We next overexpressed IGF1 in VIP neurons by injecting *Vip-cre* mice with an AAV construct that drives expression of an epitope-tagged version of IGF1 together with EGFP in a Cre-dependent manner (Fig. 3k and Extended Data Fig. 7b, c) and assessed the effect on mIPSCs and mEPSCs (Fig. 3l–o). We find that when overexpressed in VIP neurons, IGF1 selectively promotes inhibition onto VIP neurons, as it has no effect on mEPSCs in these cells. Likewise, ectopic expression of IGF1 in SST and excitatory neurons (by intracortical injections into *Sst*- or *Emx1-cre* mice, respectively; Extended Data Fig. 7d–g) leads to a similar increase in mIPSC frequency in these cells. These findings raise the possibility that the selective expression of *Igf1* in VIP neurons is required for the proper organization and function of cortical circuits, as aberrant IGF1 expression could enhance inhibition indiscriminately within cortical circuits by signalling through IGF1 receptors that are ubiquitously expressed in these neurons (Extended Data Fig. 7h–j).

The change in mIPSC frequency upon *Igf1* knockdown in VIP neurons could reflect a change in the presynaptic probability of release and/or a reduction in inhibitory synapse number and/or strength. By paired-pulse stimulation we find that *Igf1* knockdown in VIP neurons does not significantly alter the probability of release of vesicles

from either inhibitory (Fig. 4a) or excitatory (Extended Data Fig. 7k) terminals that synapse onto VIP neurons. To test evoked inhibition, we co-injected *Vip-cre* mice with either *Igf1* or control shRNA AAVs and an AAV encoding the excitatory light-activated ion channel *ReachR*¹⁷. Performing paired voltage clamp recordings from eGFP-positive VIP neurons and neighbouring pyramidal cells to control for variation in stimulation intensity, we found that the strength of light-evoked inhibition onto VIP neurons is decreased when *Igf1* expression is knocked down in VIP neurons (Fig. 4b). These experiments suggest that the primary site of IGF1 action is post-synaptic and indicate that experience-dependent activation of *Igf1* expression increases the number and/or strength of functional inhibitory synapses that form on VIP neurons. To test whether this IGF1-dependent decrease in inhibition alters the frequency of action potentials in these neurons, we performed cell-attached recordings from eGFP-labelled VIP neurons expressing control or *Igf1* shRNAs. We find that VIP neurons lacking IGF1 fire action potentials at a significantly higher rate than controls (Fig. 4c). Given that VIP neurons disinhibit cortical circuits, it seems likely that this decreased firing of VIP neurons might alter how the cortex responds to sensory experience. To begin to investigate this possibility, we next assessed the effect of knocking down *Igf1* expression on visual cortex plasticity.

Cortical inhibition regulates ocular dominance (OD) plasticity^{1,18} and visual acuity¹⁹, and hyper-activation of VIP neurons drives a form of adult cortical plasticity²⁰. To determine whether knocking down *Igf1* expression in VIP neurons affects visual cortex function, we injected control or *Igf1* shRNA AAVs into the binocular zone of visual cortices of P18 *Vip-cre* mice and recorded visual-evoked potentials between P28 and P32 (Fig. 4d and Extended Data Fig. 8a). Stimulation of the contralateral or ipsilateral eye with gratings at low spatial frequency elicited robust visual-evoked potentials both under control and *Igf1*-knockdown conditions (Extended Data Fig. 8b–d). Furthermore, the ratio between the contralateral and ipsilateral eye's response (C:I ratio) was similar in the presence or absence of *Igf1* (Extended Data Fig. 8e), indicating that basic visual cortex function is not obviously disrupted

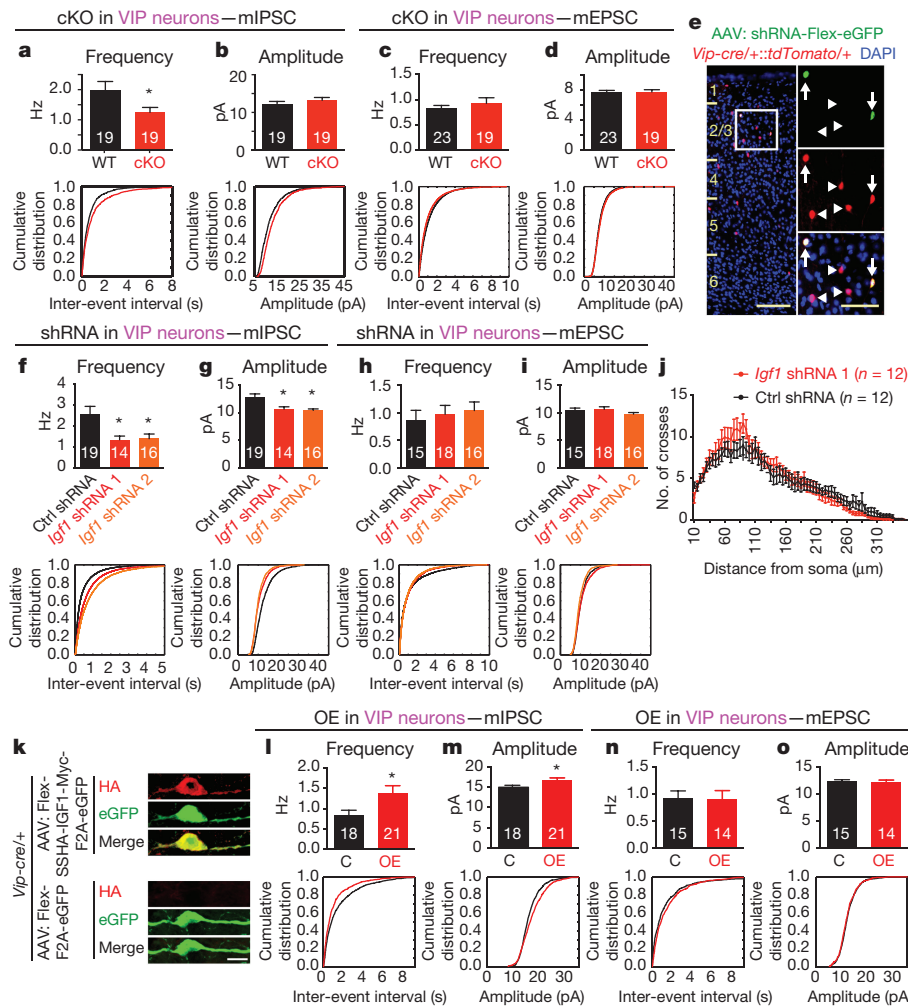


Figure 3 | IGF1 promotes inhibitory inputs to VIP neurons in a cell-autonomous manner. **a–d**, Bar graph and cumulative distribution of the frequency and inter-event intervals of mIPSCs or mEPSCs recorded from *Igf1* wild-type (WT) or conditional-knockout (cKO) VIP neurons (mIPSC frequency, $P=0.046$; amplitude, $P=0.3$; mEPSC frequency, $P=0.44$; amplitude, $P=0.9$, Mann–Whitney *U*-test). **e**, Example image of sparsely infected VIP neurons upon injection of AAV-shRNA-hUbc-Flex-eGFP into mice expressing tdTomato in all VIP neurons (white box indicates the magnified area; arrows indicate infected VIP neurons; arrowheads indicate non-infected VIP neurons; scale bars, 100 μ m in main image; 50 μ m in magnification). **f–i**, Bar graph and cumulative distribution of mIPSC/mEPSC frequency, inter-event interval and amplitude recorded from VIP neurons sparsely infected with control or *Igf1* shRNAs (mIPSC frequency: shRNA 1, $P=0.05$; shRNA 2, $P=0.042$; mIPSC amplitude: shRNA 1, $P=0.004$; shRNA 2, $P=0.001$; mEPSC frequency, shRNA 1,

$P=0.13$; shRNA 2, $P=0.07$; mEPSC amplitude: shRNA 1, $P=0.77$; shRNA 2, $P=0.44$, Mann–Whitney *U*-test). **j**, Sholl analyses of VIP neurons infected with control or *Igf1* shRNA ($P=0.76$, two-way repeated-measures ANOVA). **k**, Expression of epitope-tagged IGF1.4 in VIP-neurons. Cortices of P3 *Vip-cre/+* mice were injected with AAVs driving Cre-dependent expression of SSHA-IGF1.4-Myc-F2A-eGFP (top) or F2A-eGFP (bottom) and stained for HA (red) and eGFP (green) (Scale bar, 10 μ m). **l–o**, Bar graphs and cumulative distribution plots showing mIPSC/mEPSC amplitude and frequency/inter-event interval in VIP neurons infected with a control AAV or an AAV over-expressing (OE) IGF1. mIPSC: amplitude, $P=0.05$; frequency, $P=0.02$; mEPSC: amplitude, $P=0.55$; frequency, $P=0.86$, Mann–Whitney *U*-test. **a–d**, **f–j**, **l–o**, Numbers inside bars indicate the number of cells recorded; * $P < 0.05$ by Mann–Whitney *U*-test.

upon *Igf1* knockdown. Remarkably, when we assessed visual acuity of the contralateral eye by increasing the spatial frequency of the gratings presented, the mice injected with AAVs expressing *Igf1* shRNA exhibited significantly increased visual acuity as compared to mice injected with control AAVs (Fig. 4g).

To test whether the effect of *Igf1* knockdown is experience-dependent, we next monocularly deprived mice for a brief period of time, beginning at the peak time of ocular dominance plasticity (that is, at P26–28, Fig. 4d). After four days of monocular deprivation, we recorded visual-evoked potentials from the visual cortex contralateral to the deprived eye and quantified the C:I ratio upon stimulation at low spatial frequency as well as the visual acuity upon stimulation of the deprived eye. Brief monocular deprivation led to a reduction in the C:I ratio in mice injected with AAVs expressing either control or *Igf1* shRNA; this is a consequence of the reduction in the contralateral response

(Extended Data Fig. 8b–e)¹⁸. Notably, when we tested visual acuity after brief monocular deprivation, both *Igf1* and control shRNA injected mice exhibited similar levels of amblyopia (that is, loss of visual acuity) in the deprived eye (Fig. 4e–g), despite the higher visual acuity in the *Igf1* shRNA injected mice that were not monocularly deprived (Fig. 4e–g). These findings indicate that VIP neuron-derived IGF1 regulates visual acuity in an experience-dependent manner and may function as a sensory-dependent brake on cortical plasticity. The observation that in response to sensory experience IGF1 in VIP neurons controls inhibition, taken together with the previous finding that experience induces BDNF in excitatory neurons to regulate excitatory–inhibitory balance^{21,22}, suggests a model in which each type of neuron within a cortical circuit expresses a unique set of experience-induced secreted factors that control specific synaptic inputs onto the neuron and plasticity within a neural circuit^{6,23}.

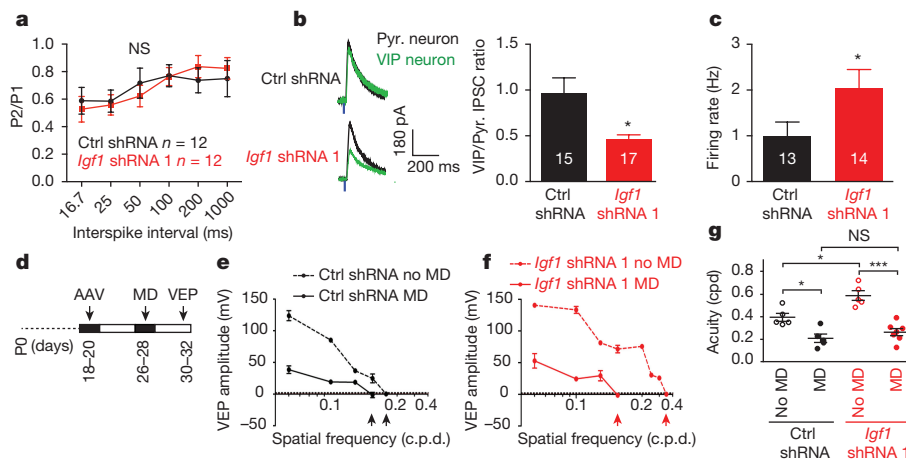


Figure 4 | VIP-neuron-derived IGF1 regulates VIP neuron function and regulates visual acuity in an experience-dependent manner. **a**, Paired-pulse recordings from VIP neurons infected with control or *Igf1* shRNA ($P=0.96$, two-way ANOVA). **b**, Left, average traces of light-evoked IPSCs (eIPSC) from paired recordings of VIP neurons infected with control or *Igf1* shRNA (green traces) and neighbouring pyramidal neurons (Pyr., black traces). Right, quantification of eIPSC amplitude of the VIP neuron after infection with AAVs expressing control or *Igf1* shRNA, normalized to the eIPSC amplitude of the paired pyramidal neuron ($P=0.01$, Mann-Whitney *U*-test). **c**, Average firing rate of VIP neurons infected with *Igf1* or control shRNA ($P=0.04$, Mann-Whitney *U*-test). **b**, **c**, Numbers inside bars indicate the number of

cells recorded. **d**, Schematic of the schedule for monocular deprivation (MD) experiments. **e**, **f**, Representative traces of visually evoked potential (VEP) amplitude as a function of spatial frequency (cycles per degree (c.p.d.)) in the contralateral visual cortex of mice that received bilateral injections of AAVs expressing *Igf1* or control shRNA into their visual cortices and were subjected to monocular deprivation or not. **g**, VIP-neuron-derived IGF1 restricts visual acuity in an experience-dependent manner. Visual acuity in mice injected with AAVs expressing *Igf1* or control shRNA with or without monocular deprivation (P24–P28; control shRNA no MD, $n=5$; control shRNA MD, $n=5$; *Igf1* shRNA no MD, $n=5$; *Igf1* shRNA MD, $n=7$; $*P<0.05$; $***P<0.0001$; NS, not significant; one-way ANOVA with Tukey's post hoc test).

Online Content Methods, along with any additional Extended Data display items and Source Data, are available in the online version of the paper; references unique to these sections appear only in the online paper.

Received 30 June 2014; accepted 29 January 2016.

Published online 9 March 2016.

- Hensch, T. K. Critical period plasticity in local cortical circuits. *Nature Rev. Neurosci.* **6**, 877–888 (2005).
- Rudy, B., Fishell, G., Lee, S. & Hjerling-Leffler, J. Three groups of interneurons account for nearly 100% of neocortical GABAergic neurons. *Dev. Neurobiol.* **71**, 45–61 (2011).
- Pfeffer, C. K., Xue, M., He, M., Huang, Z. J. & Scanziani, M. Inhibition of inhibition in visual cortex: the logic of connections between molecularly distinct interneurons. *Nature Neurosci.* **16**, 1068–1076 (2013).
- Lee, S., Kruglikov, I., Huang, Z. J., Fishell, G. & Rudy, B. A disinhibitory circuit mediates motor integration in the somatosensory cortex. *Nature Neurosci.* **16**, 1662–1670 (2013).
- Pi, H.-J. *et al.* Cortical interneurons that specialize in disinhibitory control. *Nature* **503**, 521–524 (2013).
- Spiegel, I. *et al.* Npas4 regulates excitatory-inhibitory balance within neural circuits through cell-type-specific gene programs. *Cell* **157**, 1216–1229 (2014).
- Majdan, M. & Shatz, C. J. Effects of visual experience on activity-dependent gene regulation in cortex. *Nature Neurosci.* **9**, 650–659 (2006).
- Sanz, E. *et al.* Cell-type-specific isolation of ribosome-associated mRNA from complex tissues. *Proc. Natl Acad. Sci. USA* **106**, 13939–13944 (2009).
- Kubota, Y. *et al.* Selective coexpression of multiple chemical markers defines discrete populations of neocortical GABAergic neurons. *Cereb. Cortex* **21**, 1803–1817 (2011).
- Bondy, C. A. Transient IGF-I gene expression during the maturation of functionally related central projection neurons. *J. Neurosci.* **11**, 3442–3455 (1991).
- Liu, J. P., Baker, J., Perkins, A. S., Robertson, E. J. & Efstratiadis, A. Mice carrying null mutations of the genes encoding insulin-like growth factor I (*Igf-1*) and type 1 IGF receptor (*Igf1r*). *Cell* **75**, 59–72 (1993).
- Cheng, C. M. *et al.* Insulin-like growth factor 1 is essential for normal dendritic growth. *J. Neurosci. Res.* **73**, 1–9 (2003).
- Cao, P., Maximov, A. & Südhof, T. C. Activity-dependent IGF-1 exocytosis is controlled by the Ca^{2+} -sensor synaptotagmin-10. *Cell* **145**, 300–311 (2011).
- Nishijima, T. *et al.* Neuronal activity drives localized blood-brain-barrier transport of serum insulin-like growth factor-I into the CNS. *Neuron* **67**, 834–846 (2010).
- Liu, J. L. *et al.* Insulin-like growth factor-I affects perinatal lethality and postnatal development in a gene dosage-dependent manner: manipulation using the *Cre/loxP* system in transgenic mice. *Mol. Endocrinol.* **12**, 1452–1462 (1998).

- Hede, M. S. *et al.* E-peptides control bioavailability of IGF-1. *PLoS ONE* **7**, e51152 (2012).
- Lin, J. Y., Knutsen, P. M., Muller, A., Kleinfeld, D. & Tsien, R. Y. ReaChR: a red-shifted variant of channelrhodopsin enables deep transcranial optogenetic excitation. *Nature Neurosci.* **16**, 1499–1508 (2013).
- Fagiolini, M. & Hensch, T. K. Inhibitory threshold for critical-period activation in primary visual cortex. *Nature* **404**, 183–186 (2000).
- Davis, M. F. *et al.* Inhibitory neuron transplantation into adult visual cortex creates a new critical period that rescues impaired vision. *Neuron* **86**, 1055–1066 (2015).
- Fu, Y., Kaneko, M., Tang, Y., Alvarez-Buylla, A. & Stryker, M. P. A cortical disinhibitory circuit for enhancing adult plasticity. *eLife* **4**, e05558 (2015).
- Hong, E. J., McCord, A. E. & Greenberg, M. E. A biological function for the neuronal activity-dependent component of Bdnf transcription in the development of cortical inhibition. *Neuron* **60**, 610–624 (2008).
- Bloodgood, B. L., Sharma, N., Browne, H. A., Trepman, A. Z. & Greenberg, M. E. The activity-dependent transcription factor NPAS4 regulates domain-specific inhibition. *Nature* **503**, 121–125 (2013).
- Turrigiano, G. Too many cooks? Intrinsic and synaptic homeostatic mechanisms in cortical circuit refinement. *Annu. Rev. Neurosci.* **34**, 89–103 (2011).

Supplementary Information is available in the online version of the paper.

Acknowledgements We thank C. Chen for help with electrophysiology experiments, E. Griffith and T. Cherry for critical reading of the manuscript, P. Zhang for managing the mouse colony and the HMS Biopolymers Facility Next-Gen Sequencing Core for their expertise in constructing Seq libraries and sequencing of the library samples. The ReachR-tdTomato construct was a gift from J. Lin, and we thank M. Li for production of the ReachR-virus. H.A. is a New York Stem Cell Robertson Investigator. This work was funded by fellowships by the Human Frontiers Science Program and the Swiss National Science Foundation (I.S.) and the National Institute of Health grants R01 NS028829 and P01 NS047572 (M.E.G.).

Author Contributions Experiments were designed by A.R.M., I.S. and M.E.G. Experiments were conducted and analysed by A.R.M., I.S., E.C., A.P., C.P.T., J.E.B., C.M.B. and D.A.H. Experiments were supervised by H.A., M.F. and M.E.G. The manuscript was prepared by A.R.M., I.S. and M.E.G.

Author Information Raw data and processed values from RiboTag-Seq have been submitted to the NCBI Gene Expression Omnibus under the accession number GSE77243. Reprints and permissions information is available at www.nature.com/reprints. The authors declare no competing financial interests. Readers are welcome to comment on the online version of the paper. Correspondence and requests for materials should be addressed to M.E.G. (Michael_Greenberg@hms.harvard.edu).

METHODS

No statistical methods were used to predetermine sample size.

Visual stimulation. For calibrating the duration of the dark housing period before light exposure, C57Bl6 wild-type mice were housed in a standard light cycle until they were placed in constant darkness for varying amounts of time before analysis at postnatal day 56. At P56, all mice were either sacrificed in the dark (dark-housed condition) or light-exposed for 1, 3, or 7.5 h before being sacrificed. The eyes of all animals were enucleated (for the dark-housed condition, enucleation was performed in the dark) before dissection of the visual cortex in the light.

For RiboTag-experiments, mice were reared in a standard light cycle and then housed in constant darkness for two weeks starting from P42; at P56, all mice were either sacrificed in the dark (dark-housed condition) or light-exposed for 1, 3, or 7.5 h before being sacrificed. Additional cohorts of mice for the 'standard' condition were housed in a standard light cycle until P56 when they were euthanized. The eyes of all animals were enucleated (for the dark-housed condition, enucleation was performed in the dark) before dissection of the visual cortex in the light.

RNA isolation, reverse transcription, qPCR analysis. Total RNA was extracted with TRIzol reagent (Sigma) according to the manufacturer's instructions, and RNA quality was assessed on a 2100 BioAnalyzer (Agilent); all RNAs were treated with DNaseI (Invitrogen) before reverse transcription. For the cloning of riboprobes, total RNA was extracted from whole adult C57Bl6 wild-type mouse brains and cDNA was prepared using SuperScript II kit (Life Technologies). For real-time quantitative PCR experiments aimed at calibrating the duration of the dark housing period, total RNA was extracted for each sample from the visual cortices of one animal. For real-time quantitative PCR experiments aimed at testing the efficacy of shRNA constructs directed against *Igf1*, total RNA was isolated from two pooled 24 wells of cultured cortical neurons for each condition. For qPCR experiments, RNA was reverse-transcribed with the High Capacity cDNA Reverse Transcription kit (Life Technologies). Real-time quantitative PCR reactions were performed on the LightCycler 480 system (Roche) with LightCycler 480 SYBR Green I Master. Reactions were run in duplicates, triplicates or quadruplicates, and β -actin (*Actb*) or β 3-tubulin (*Tubb3*) levels were used as an endogenous control for normalization using the $\Delta\Delta C_t$ method²⁴. Real-time PCR primers were designed using the Universal ProbeLibrary (Roche) as exon-spanning whenever possible and answered the following criteria: linear amplification over three orders of magnitude of target concentration, no amplification product in control samples that were not reverse-transcribed (that is, control for contamination with genomic DNA), no amplification product in control samples where no template was added (that is, control for primer dimers), amplification of one singular product as determined by melt-curve analysis and analysis of the product in agarose gel electrophoresis and sequencing of the PCR product. The qPCR primers used in this study are listed in Supplementary Table 6.

For analysis of light-induced gene expression in wild-type mice, the gene expression levels were analysed in four mice (two males and two females) at each time point. The data were calculated as fold change relative to the average of the overnight dark-housed condition and normalized to the average of the maximally induced time point. Data in figures represent the mean and s.e.m. of four mice.

For assessing *Igf1* levels in cortical cultures infected with shRNA-expressing lentiviral constructs, qPCRs were performed in quadruplicates for each condition and fold changes were calculated relative to the non-infected non-stimulated cultures. Data were normalized to the maximally induced condition in each biological replicate, and data in figures represent the mean and s.e.m. of three biological replicates.

RiboTag-purifications, RiboTag-qPCR and RiboTag-seq. Immunoprecipitation and purification of ribosome associated RNA was performed essentially as described^{6,8}, with minor modifications: lysis of the samples was performed in the presence 10 mM Ribonucleoside Vanadyl Complex (NEB, Ipswich, MA), and immunoprecipitation was performed with a different anti-HA antibody (HA-7, 12 μ g per immunoprecipitation, Sigma). In brief, the visual cortices were dissected, flash frozen in liquid nitrogen and then kept at -80°C until further processing. Visual cortices from three individual animals (each sample contained both male and female animals) were pooled for each biological replicate, and three biological replicates were performed. After lysis of the tissues and before immunoprecipitation, a small fraction of lysate of each sample (that is, 'input') was set aside and total RNA was extracted with TRIzol reagent followed by the RNEasy Micro Kit's procedure (Qiagen, Valencia, California). After immunoprecipitation of the ribosome-associated RNAs, RNA quality was assessed on a 2100 BioAnalyzer (Agilent, Palo Alto, California) and RNA amounts were quantified using the Qubit 2.0 Fluorometer (Life Technologies). Only samples with RIN numbers above 8.0 were considered for analysis by qPCR and RNA-seq. For all RNA samples of sufficient integrity, 5–10 ng of RNA were SPIA-amplified with the Ovation RNA Amplification System V2 (NuGEN, San Carlos, California), yielding typically 5–8 μ g of cDNA per sample.

Quantitative RT-PCR was performed as described above and relative expression levels were determined in every experiment by normalizing the Ct-values to those of beta-Actin (*Actb*) from the 0 h input using the $\Delta\Delta C_t$ method²⁴. To determine the fold-enrichment (IP/Input), the actin-normalized expression levels for every time point of every biological replicate were averaged, and the grand averages from the IP and Input were divided to find the IP/Input ratio. To calculate fold-induction for each biological replicate, each time point was divided by the maximal value occurring in that biological replicate, such that the maximal value was set to 1 in each biological replicate. The mean and standard error were calculated at each time point from these normalized values. All samples were analysed by qPCR for purity and light-induced gene expression before analysis by high throughput sequencing. **RNA-seq and analysis.** SPIA-amplified samples from RiboTag-immunoprecipitated fractions for each of the five stimulus conditions and each of the five Cre lines were prepared as described above and processed in triplicate (75 samples total). For preparing sequencing libraries, 2 μ g of each amplified cDNA were fragmented to a length of 200–400 bp using a Covaris S2 sonicator (Acoustic Wave Instruments) using the following parameters: duty cycle: 10%, intensity: 5, cycles per burst: 200, time: 60 s, total time: 5 min. After validating the fragment length of the sonicated cDNA using a 2100 BioAnalyzer (Agilent, Palo Alto, California), 2 μ g of the fragmented cDNA were used for sequencing library preparation using the PrepX DNA kit on an Apollo 324 robot (IntegenX). The quality of completed sequencing libraries was assessed using a 2100 BioAnalyzer (Agilent, Palo Alto, California) and the completed libraries were sequenced on an Illumina HiSeq 2000 instrument, following the manufacturer's standard protocols for single-end 50 bp sequencing with single index reads. Sequencing typically yielded 30–80 million usable non-strand-specific reads per IP sample. Reads were mapped to the mm9 genome using TopHat (v.2.0.13) and Bowtie (2.1.0.0)²⁵. On average, ~70% of mapped IP reads were uniquely mapped to the mm9 genome allowing for 0 mismatches and were therefore assignable to genic features (one RiboTag-seq library (*Sst-cre*, standard-housing, biological replicate 2) was excluded from analysis due to low mappability). Values from all IP libraries were normalized using Cuffnorm (v.2.2.1), and values from the Cuffnorm output file 'genes-Count_Table' (normalized reads) were taken as a proxy for gene expression. *P* values were generated for each Cre line for each dark–light conditions using Cuffdiff (v.2.2.1) using the time series (-T) flag based on three biological replicates.

Identification and classification of experience-regulated transcripts. To identify transcripts regulated by visual experience, for each biological replicate of each Cre line, the fold change in normalized reads was calculated for each gene at every time point (dark-housed/standard-housed, 1 h light/dark-housed, 3 h light/dark-housed; 7.5 h light/dark-housed). Genes were flagged as experience-regulated in a given Cre line if they met the following conditions in at least one sample: (1) *P* value <0.005 , (2) mean fold change of twofold or greater, (3) fold changes of 2 or higher in 2 of 3 biological replicates, (4) the mean expression value in at least one sample must be above absolute expression threshold (set at the 40th percentile of all observed values).

To determine in which Cre lines genes were regulated by experience, genes were simply classified according to the above criteria. However, for this analysis we excluded the *Gad2-cre* line, since *Pv-*, *Sst-* and *Vip-cre* all label subsets of the neurons labelled by *Gad2-cre*. However, we did detect genes regulated solely in *Gad2-cre*, but no other Cre lines; we reasoned that these genes are probably regulated by experience in a population of 5HT3aR⁺/VIP⁻ neurons that are contained in *Gad2-cre* but none of the other Cre lines.

We classified the set of experience-regulated genes into categories 'early', 'late', and 'long-term' based on the fastest kinetics observed. When genes were found to be elevated and/or suppressed at multiple time points, we assigned them to the categories based on the most rapid observed change. For example, while *Fos* levels are elevated over dark housing at 1, 3 and 7.5 h of light exposure and suppressed after two weeks of dark housing, *Fos* is classified as 'early-up' because it is elevated at 1 h after light exposure.

Linkage analysis. All linkage analysis was performed using the 'single' method and 'Cytblock' metric using Matlab's linkage function. To determine the branch-order significance of the cladogram resulting from clustering of the 602 experience-regulated genes, we generated 1,000 cladograms from 602 sets of random expressed genes (including experience-regulated genes, with replacement) and asked how often we generated a cladogram with an identical branch order at the level of the Cre lines. Only 11 sets of 1,000 random genes sets generated an identical tree. For the purposes of this analysis, we only compared the branches above the level of the individual Cre line.

Identification of cell-type-specific transcripts. To identify cell-type-enriched transcripts, an enrichment score was calculated for every transcript in every Cre line for each biological replicate. This enrichment score was calculated by dividing the maximum expression value observed in a given Cre line by the maximum expression value observed across all conditions for all other Cre lines

(GABAergic subtypes were not required to be enriched above *Gad2-cre*). The enrichment scores for a set of known cell-type-specific genes were evaluated (*Vglut1*, *Tbr1*, *Pvalb*, *Sst*, *Vip*), and our threshold was set at the enrichment score of the cell-type-specific gene with the lowest score (*Slc17a7/Vglut1*, at 5.5-fold-enriched in *Emx1-cre*). Transcripts were considered to be expressed in a cell-type-specific manner (or 'highly enriched') in a given Cre line if their mean enrichment score was above this threshold and if the enrichment score exceeded this threshold in 2 out of 3 biological replicates.

Cloning of riboprobes, knockdown and expression constructs. Cloning of all constructs was done using standard cloning techniques, and the integrity of all cloned constructs was validated by DNA sequencing. Templates for the riboprobes for *Igf1*, *Gad1*, *Pvalb*, *Sst* and *Vip* were prepared by PCR-amplification of cDNA fragments generated from total RNA isolated from adult C57Bl6 mouse brains (see Supplementary Table 7 for primer sequences) and cloning of the respective PCR fragments into the pBlueScript II vector (Agilent Technologies).

Lentiviral shRNA constructs were generated by cloning shRNA stem loop sequences against *Igf1* (*Igf1* shRNA 1: GGTGGATGCTCTTCAGTTC; *Igf1* shRNA 2: TGAGGAGACTGGAGATGTA) and Luciferase (*Luc*, control: ACTTACGCTGAGTACTTCG) into a modified version of pLentiLox3.7²⁶ in which the CMV promoter driving the expression of eGFP was replaced with an hUbc promoter and in which the *loxP* sites surrounding the hUbc-eGFP cassette were removed. The loop sequence used in these shRNA constructs is based on miR-25 (CCTCTCAACTGG)²⁷. shRNA-expressing AAV-constructs (pAAV-U6-shRNA-hUbc-Flex-eGFP) were made by first replacing the Flex-GFP-Gephyrin cassette in pAAV-Flex-GFP-Gephyrin²² with a Flex-eGFP cassette (resulting in pAAV-hUbc-Flex-eGFP) and then transferring the U6-shRNA cassettes from the pLentiLox constructs to pAAV-hUbc-Flex-eGFP.

AAV constructs for the Cre-conditional co-expression of epitope-tagged IGF1.4 and eGFP or of eGFP alone were cloned by synthesizing the gBlocks (Integrated DNA Technologies) and using the gBlocks as templates for PCR amplification; the respective PCR products were then cloned into the pAAV-hUbc-Flex-eGFP (see above) by replacing the eGFP with the respective insert. This strategy yielded plasmids termed pAAV-hUbc-Flex-SSHA-IGF1.4-Myc-F2A-eGFP and pAAV-hUbc-Flex-F2A-eGFP, whereby the Cre-dependent inserts were driven by a human ubiquitin promoter (hUbc). The sequence for *Igf1.4* was based on NM_00111275 (base pairs 277–752) and was modified in the following way: an HA epitope (TATCCtTATGATGTTCCAGATTATGCT) was inserted in frame between the *Igf1.4* signal sequence and the beginning of the coding sequencing (cds) of *Igf1.4*. *Igf1.4* was rendered resistant to the shRNA against *Igf1* by introducing silent mutations into the target sequences specified above (sh1: TGTTGACGGCTCCAATTT; sh2: TACGCCGGTTAGAAATGTA) and the following tags were inserted in frame 3' to the *Igf1.4* coding sequencing: Myc epitope (GAACAAAACACTCATCTCAGAAGAGGATCTG), Furin cleavage site (CGGGCCAAGCGG) and a 2A peptide (GGCAGTGGAGAGGGCAGAGGA AGTCTTCTAACATGCGGTGAGTGGAGGAGAATCCCGGCCCT). The sequence for eGFP was based on the published sequence of eGFP. For pAAV-hUbc-Flex-F2A-eGFP a gBlock was synthesized containing the Furin cleavage site followed by the 2A site and eGFP. Detailed sequences are available upon request.

Double-fluorescent ISH. For double-fluorescent *in situ* hybridization (FISH), wild-type C57Bl6 mice were dark-housed and light-exposed for 7.5 h as described above. After light exposure, the brains were dissected and fresh frozen in Tissue-Tek Cryo-OCT compound (Fisher Scientific) on dry ice and stored at -80°C until use.

FISH for *Igf1* was essentially done as described^{28,29}: riboprobes were prepared by *in vitro* transcription of linearized plasmids containing the template of the respective probe. Riboprobes for *Igf1* were labelled with UTP-11-Digoxigenin, while the riboprobes for the subtype markers (*Gad1*, *Pvalb*, *Sst*, *Vip*) were labelled with UTP-12-Fluorescein (Roche); all riboprobes were hydrolyzed to lengths of 200–400 bp after synthesis and validated for labelling with Digoxigenin or Fluorescein. For *in situ* hybridization, coronal sections (20 μm thick) of the visual cortex were cut on a cryostat and fixed in 4% paraformaldehyde for 10 min. Endogenous peroxidases were inactivated by treating the sections for 15 min in 0.3% H_2O_2 in PBS, and acetylation was performed as described. Pre-hybridization was done overnight at room temperature, and hybridization was performed under stringent conditions at 71.5°C . Following hybridization, stringency washes in SSC were performed as described at 65°C . For immunological detection of the first probe (*Igf1*), the tissue was first treated with a blocking step for 1 h in blocking buffer (B2) at room temperature before the anti-Digoxigenin-POD antibody (Roche) was applied at a concentration of 1:1000 in blocking buffer for 1 h at room temperature. Following three washes in buffer B1 and an additional wash in buffer TNT (0.1 M Tris-HCl pH 7.5, 0.15 M NaCl, 0.05% Tween20), the *Igf1* probe was detected by exposing the sections at room temperature in the dark for 20 min to TSA Plus Cy3 reagent (Perkin Elmer) diluted 1:100 in TSA working solution, after which the sections

were washed three times in TNT buffer. Before the immunological detection of the second probe, the peroxidases for detecting the first probe were inactivated by treating the sections for 30 min with 3% H_2O_2 , followed by three washes in PBS. After an additional blocking step in blocking buffer for 1 h at room temperature, the anti-fluorescein-POD antibody (Roche) was applied at a concentration of 1:1000 in blocking buffer overnight at 4°C . Following three washes in buffer B1 and an additional wash in buffer TNT, the probes of the subtype markers were detected by exposing the sections at room temperature in the dark for 15 min to TSA Plus Cy5 reagent (Perkin Elmer) diluted 1:100 in TSA working solution, after which the sections were washed three times in TNT buffer. Finally, the sections were counterstained with DAPI (4',6-diamidino-2-phenylindole, Molecular Probes) and mounted using Fluoromount-G (Southern Biotech). In each experiment, controls for hybridization specificity were included (sense probe for *Igf1*) as well as controls for ensuring the specificity of the immunological detection of the digoxigenin- and fluorescein-labelled riboprobes.

FISH for *Crh*, *Prok2* and *Fbln2* was done using the RNAscope system (Advanced Cell Diagnostic); this was necessary since no reliable signal could be detected with the method described above for *Igf1* FISH using DIG-labelled riboprobes. RNAscope probes for all genes were synthesized by ACD and all experiments were done according to the ACD's protocol for fresh frozen brain sections.

For quantifying of the expression pattern of all genes of interest (GOI, that is, *Igf1*, *Crh* and *Prok2*; *Fbln2* could not be detected reliably), the visual cortices in each section were imaged on a Zeiss Axio Imager microscope with a $10\times$ objective and 3×5 fields-of-view were 'stitched' into one compound image; in all cases, image exposures were kept constant throughout a given experiment for each channel. Compound images of each visual cortex were then imported to Photoshop, and additional layers were created for each probe (that is, one layer for the GOI and one layer for the subtype marker in each compound image). The cells positive for each probe were then marked with a dot in the new respective layer by two independent investigators in a blinded manner (one investigator marking GOI-positive cells and the other investigator marking subtype-marker-positive cells). Finally, the layers containing the dots of the identified positive cells were compiled into a separate image file together with the DAPI-layer and imported into ImageJ. In ImageJ, the images were analysed in a blinded manner by defining the visual cortex and its layers as regions of interest (ROI) based on the DAPI staining and quantifying the number of cells positive for either one or both markers per ROI. For each combination of probes (GOI together with each of the subtype markers), two visual cortices from four animals were analysed (a total of eight visual cortices for each combination).

Virus production and neuronal cultures. Concentrated lentiviral stocks were prepared and titrated essentially as described³⁰. AAV stocks were prepared at the University of North Carolina (UNC) Vector Core and at the Children's Hospital Boston Vector Core; see also Supplementary Table 8 for further details on AAV stocks.

Primary cultures of cortical neurons were prepared from E16.5 mouse embryos as described⁶. In brief, 3×10^5 neurons per well were plated in 24-well dishes coated with poly-D-lysine ($20\mu\text{g ml}^{-1}$) and laminin ($3.4\mu\text{g ml}^{-1}$). Cultures were maintained in neurobasal medium supplemented with B27 (Invitrogen), 1 mM L-glutamine, and 100 U ml⁻¹ penicillin/streptomycin, and one-third of the media in each well was replaced every other day. For testing of viral shRNA constructs, the cultures were infected at DIV 3 with concentrated viral stocks for 5 h at an MOI of 6. After infection, the cultures were washed twice in plain neurobasal medium after which the conditioned medium was returned to the dish and the cultures were continued to be maintained as described. At DIV 7, neuronal cultures were treated overnight with 1 μM TTX and 100 μM AP-5 to silence spontaneous activity before the cultures were depolarized at DIV 8 with 55 mM extracellular KCl as described⁶ and lysed in TRIzol after 6 h of stimulation.

Western blot for testing of IGF1 constructs and ELISA for determining serum IGF1 levels. HEK293T cells were used for testing the expression and the biological activity of the epitope-tagged IGF1.4 constructs. HEK293T cells were cultured in DMEM (Life Sciences) containing 10% FCS and penicillin/streptomycin. Cells were transfected using lipofectamine (Life Technologies) and 18 h post transfection, the medium was replaced with DMEM containing 0.1% FCS; 42 h post transfection, the conditioned media were collected, spun down to remove cell debris and used immediately for stimulating non-transfected HEK293T that were serum starved for 3 days in DMEM containing 0.1% FCS. The conditioned media were applied to the serum starved cells for 15 min at 37°C after which the cells were lysed in boiling SDS sample buffer and subjected to Western blot analysis essentially as described^{6,31}. For detecting the (phosphorylated) IGF1-receptor, the following antibodies were used: anti-IGF1-receptor- β (D23H3) XP Rabbit mAb (#9750, Cell Signaling, 1:1000) and anti-phospho-IGF1-receptor- β (Tyr1135/1136)/Insulin Receptor β (Tyr1150/1151) (19H7) Rabbit mAb (#3024, Cell Signaling, 1:1000). For determining serum IGF1 levels, we used the IGF1 Quantikine ELISA kit (R&D

Systems), following the manufacturer's instructions (P3 *Vip-cre* heterozygous pups were injected intracortically with the respective AAV and bled at P20).

Perfusions, immunohistochemistry and morphological analysis of IGF1 cKO visual cortices. Mice were anaesthetized with 10% ketamine and 1% xylazine in PBS by intraperitoneal injection. When fully anaesthetized, the animals were transcardially perfused with ice-cold PBS for 5 minutes followed by 15 minutes of cold 4% PFA in PBS. Brains were dissected and post-fixed for one hour at 4°C in 4% PFA, followed by three washes (each for 30 min) in cold PBS, and cryoprotection overnight in 20% sucrose in PBS at 4°C. The following day, brains were placed in Tissue-Tek Cryo-OCT compound (Fisher Scientific), frozen on dry ice and stored at -80°C . Coronal sections (20 μm thick) of the visual cortices were subsequently cut using a Leica CM1950 cryostat and used for subsequent experiments.

For immunolabelling, the slides were blocked for 1 h with PBS containing 5% normal goat serum and 0.1% Triton X-100 (blocking solution). The samples were incubated overnight with different primary antibodies diluted in blocking solution, washed three times with PBS and then incubated for 45 min at room temperature with secondary antibodies and/or Hoechst stain (ThermoFisher Scientific). Slides were mounted in FluoromountG (Southern Biotech) and imaged on a Zeiss Axio Imager microscope. The following antibodies were used: mouse anti-HA (HA-7, Sigma; 1:1000), chicken anti-GFP (GFP-1020, Aves labs; 1:1500), goat anti-mouse IgG (H+L) Alexa Fluor 488 (Highly Cross-Adsorbed, Life Technologies; 1:1,000), goat anti-chicken IgY (H+L) Alexa Fluor 488 (Life Technologies; 1:1,000).

For analysing the brains of *Igfl1 Vip-cre* WT and cKO mice, brains of three-week-old WT and cKO littermates were placed on the same slide to minimize variation. After cryosectioning, the slides were either counterstained immediately or stored at -20°C before they were counterstained and imaged. Counterstaining was done with DAPI (4',6-diamidino-2-phenylindole, Molecular Probes) in PBS for 15–30 min at room temperature, after which the sections were washed once in PBS and mounted in Fluoromount-G (SouthernBiotech). For cell counting experiments, coronal visual cortex sections were imaged using a Zeiss Axio Imager microscope with a 10 \times objective and typically, 3 \times 5 fields-of-view were 'stitched' into one compound image. In all cases, image exposures were kept constant throughout a given experiment for each channel. Custom ImageJ and MATLAB macros were used to quantify the area of each cortical layer, the number tdTomato-positive cells per layer, and the size of tdTomato-positive cells. Briefly, regions of interest (ROI) encompassing the visual cortex and its layers were defined based on the DAPI counterstaining. While the width of these ROIs was kept constant throughout the analysis of all sections, the height of the ROIs was adjusted in each image according to the DAPI counterstaining in each section and the areas of each layer in each section were recorded. For analysing the number and soma size of tdTomato-positive cells in each layer, a threshold for each channel was determined based on multiple user-defined negative regions. Channels were thresholded and binarized, and a mask of each channel was created. The number of tdTomato-positive cells was determined by taking the logical AND of the DAPI and tdTomato channel masks and counting the number of components greater than 4 pixels in size in the double overlap of the masks of the two channels in each layer ROI. The soma size was calculated as the area of these double-overlapping components. Three animals per genotype and 4–6 visual cortex sections per animal were analysed, and these data were used to determine the mean and s.e.m. of the values reported for each genotype.

Stereotaxically guided surgery and intra-cortical injections of AAV constructs. All surgeries were performed according to protocols approved by the Harvard University Standing Committee on Animal Care and were in accordance with federal guidelines. Surgeries were performed on mice between P14 and P15. Animals were deeply anaesthetized by inhalation of isoflurane (initially 3–5% in O_2 , maintained with 1–2%) and secured in the stereotaxic apparatus (Kopf). Animal temperature was maintained at 37°C. The fur was shaved and scalp cleaned with betadine and 100% ethanol three times before an incision was made to expose the skull. Injections into the visual cortex were made by drilling a ~ 0.5 mm burr hole (approximately 2.7 mm lateral, 0.5 mm anterior to lambda) through the skull, inserting a glass pipette to a depth of 200–400 μm and injecting 250 nl of the respective AAV construct at a rate of 100 nl min^{-1} . Five minutes post-injection, the glass pipette was retracted, the scalp sutured and the mouse returned to its home cage. All animals were monitored for at least one hour post-surgery and at 12 h intervals for the next 5 days. Post-operatively, analgesic (flunixin, 2.5 mg per kg) was administered at 12 h intervals for 72 h.

For neonatal injections, pups post-natal day 3–5 were anaesthetized on ice for 2–3 min, and secured to a stage where their head was supported using a clay mould using standard lab tape. A bevelled glass pipette was lowered into visual cortex (approximately 2 mm lateral, 0.2 mm anterior to lambda), and 50 nl of the respective AAV virus was injected at a rate of 23 nl sec^{-1} . Injections were made into eight sites (four on each hemisphere), and the mouse was then allowed to recover on a 37°C warm plate before being returned to the home cage.

For bilateral stereotaxic intra-cortical injections of AAV constructs for visual plasticity experiments, surgeries were performed on mice between P18 and P20. Animals were anaesthetized with isoflurane gas (1–2% in O_2), and body temperature was maintained at around 37°C with a heating pad during surgery. The head was held in place by standard mouse stereotaxic frame. The fur was shaved and scalp cleaned with betadine and 100% ethanol three times before an incision was made to expose the skull. Burr holes were drilled into the skull at the point of injection guided by stereotaxic coordinates and blood vessel patterns (approximately 2 mm and 2.7 mm lateral, 0.5 mm anterior to lambda) on both hemispheres. A 28-gauge Hamilton syringe (701RN) was inserted to a depth of 200–300 μm and 250 nl of the respective AAV construct was injected at the rate of 50 nl min^{-1} . Five minutes post-injection, the Hamilton syringe was retracted, the scalp sutured and the mouse returned to its home cage. All animals were monitored for at least one hour post-surgery. Post-operatively, analgesic (meloxicam, 5–10 mg kg^{-1}) was administered every 24 h for 2 days.

Electrophysiology. Coronal sections (300 μm thick) containing the primary visual cortex were cut from P19–P21 mice using a Leica VT1000S vibratome in ice-cold choline dissection media (25 mM NaHCO_3 , 1.25 mM NaH_2PO_4 , 2.5 mM KCl, 7 mM MgCl_2 , 25 mM glucose, 0.5 mM CaCl_2 , 110 mM choline chloride, 11.6 mM ascorbic acid, 3.1 mM pyruvic acid). Slices were incubated in artificial cerebral spinal fluid (ACSF, contains 127 mM NaCl, 25 mM NaHCO_3 , 1.25 mM NaH_2PO_4 , 2.5 mM KCl, 2.5 mM CaCl_2 , 1 mM MgCl_2 , 25 mM glucose) at 32°C for 30 min immediately after cutting, and subsequently at room temperature. All solutions were saturated with 95% O_2 /5% CO_2 , and slices were used within 6 h of preparation. Whole-cell voltage-clamp recordings were performed in ACSF at room temperature from neurons in primary visual cortex that were identified under fluorescent and DIC optics. Recording pipettes were pulled from borosilicate glass capillary tubing with filaments using a P-1000 micropipette puller (Sutter Instruments) and yielded tips of 2–5.5 M Ω resistance. All experiments were recorded with pipettes filled with 135 mM caesium methanesulfonate, 15 mM HEPES, 0.5 mM EGTA, 5 mM TEA-Cl, 1 mM MgCl_2 , 0.16 mM CaCl_2 , 2 mM Mg-ATP, 0.3 mM Na-GTP, 10 mM phosphocreatine (Tris), and 2 mM QX-314-Cl. Osmolarity and pH were adjusted to 310 mOsm and 7.3 with Millipore water and CsOH, respectively. Recordings were sampled at 20 kHz and filtered at 2 kHz. mEPSCs were isolated by holding neurons at -70 mV and exposing them to 0.5 μM tetrodotoxin, 50 μM picrotoxin and 25 μM cyclothiazide and were blocked by application of 25 μM NBQX and 50 μM CPP. mIPSCs were isolated by holding neurons at 0 mV and exposing them to 0.5 μM tetrodotoxin, 25 μM NBQX, and 50 μM CPP and were blocked by 50 μM picrotoxin. Data were acquired using either Clampex10 or custom MATLAB software, using either an Axopatch 200B or Multiclamp 700B amplifier, and digitized with a DigiData 1440 data acquisition board (Axon Instruments) or a PCIe-6323 (National Instruments). For measuring miniature postsynaptic currents (minis), cells were allowed to stabilize for at least two minutes.

For paired pulse experiments, no drugs were used in the ACSF. A stimulating electrode (ISO-Flex, A.M.P.I.) was positioned approximately 100 μm below the cell, and 0.1 ms electrical pulses were given while adjusting the stimulus intensity and electrode position until the first pulse was between 100 and 500 pA. Inter-stimulus interval was varied and 10 s elapsed between each sweep. Pulse amplitudes were obtained from average sweeps of at least ten trials. Cells were held at 0 mV to record IPSCs and -70 mV to record EPSCs.

For evoked IPSCs, no drugs were used in the ACSF. Simultaneous paired whole-cell recordings were obtained from an eGFP-expressing VIP neuron and a morphologically identified pyramidal neuron located not more than five cell bodies away from the VIP neuron. Both cells were held at 0 mV, and a 5 ms light pulse from a blue LED (Thorlabs) was used to evoke IPSCs. Light intensity and the objective position were varied until the VIP neuron IPSC amplitude was between 200 and 500 pA. Average light power at 470 nm varied from between 0.3 and 0.7 mW over the course of the experiment. Reported ratios were obtained by dividing IPSC amplitudes obtained from an average trace of at least ten trials.

For electrophysiology experiments, n was set to min $n = 10$ to detect 20% effect size with power 0.95. For experiments to determine average firing rate of VIP neurons, a modified ACSF that promotes increased action potential firing was used containing, 3.5 mM KCl and 0.8 mM CaCl_2 . Cell-attached patch recordings were obtained from eGFP-positive cells. Cells that did not fire an action potential in the first 30 s of recording were discarded, and recordings were maintained for at least 30 ten-second sweeps. Average firing rate was determined from the first sweep to the last recorded sweep in which an action potential occurred.

Miniature IPSC and EPSC data were analysed using Axograph X. Events were identified using a variable amplitude template-based strategy. Templates for each event type were defined as follows: mEPSC: 0.25 ms rise time, 3 ms decay τ , amplitude threshold of $-3 \times$ s.d. local noise; mIPSC: 1 ms rise time, 50 ms decay τ , amplitude threshold of $2.5 \times$ s.d. local noise. Local noise was determined by calculating the standard deviation of the current in a 5 ms window before event rise onset.

Templates lengths extended 25 ms after rise onset in the case of mEPSCs and 50 ms after rise onset in the case of mIPSCs. Events were discarded if they had a rise time outside the range of 0–3 ms. Statistical significance for all recorded parameters between genotypes was evaluated using a Mann–Whitney *U*-test on the mean values from individual neurons in a given experiment.

Minis were additionally evaluated for significance using both a Kolmogorov–Smirnov test (KS test) and Monte Carlo test. For these tests, 50 random minis were sampled from each neuron in each condition to obtain a continuous distribution for each condition that equally weighted each cell in that condition; these distributions are the data shown in the cumulative distribution graphs. One hundred random events were randomly sampled from these distributions for a KS test; and for Monte Carlo tests, 100 random events were randomly sampled from each distribution 1,000 times (with replacement), and the means were compared. All significant differences in mini amplitude and frequency were found to be significant by Monte Carlo test, KS test, and Mann–Whitney *U*-test of cell means. Since the Mann–Whitney test was found to be the most stringent test, the *P* values from Mann–Whitney tests are reported. All data was analysed blind to genotype or experimental condition. In all conditions, series resistance, holding potential, cell capacitance, and input resistance were recorded and were not found to be significantly different except where noted. Statistical tests were performed using Graphpad Prism and MATLAB.

Sholl analysis. VIP neurons were filled with a patch pipette containing 1% Alexa 647 Hydrazide and the internal solution was allowed to dialyze for at least 30 min before slices were fixed in 4% paraformaldehyde for 1 h at room temperature. Slices were then washed three times for 30 min in PBS before slices were mounted in Fluormount-G (Southern Biotech). Images were acquired using a Zeiss Axio Imager microscope with a 20× objective with the use of an Apotome (Zeiss). Neurons were reconstructed using NeuronJ (ImageJ), and Sholl analysis was performed using a custom script in MATLAB.

Monocular deprivation (MD) procedure. Eyelids were trimmed and sutured under isoflurane anaesthesia (1–2% in O₂) as previously described³¹. The integrity of the suture was checked daily and mice were used only if the eyelids remained closed throughout the duration of the deprivation period. One eye was closed for 4 days starting between P26 to P28. The eyelids were reopened immediately before recording, and the pupil was checked for clarity.

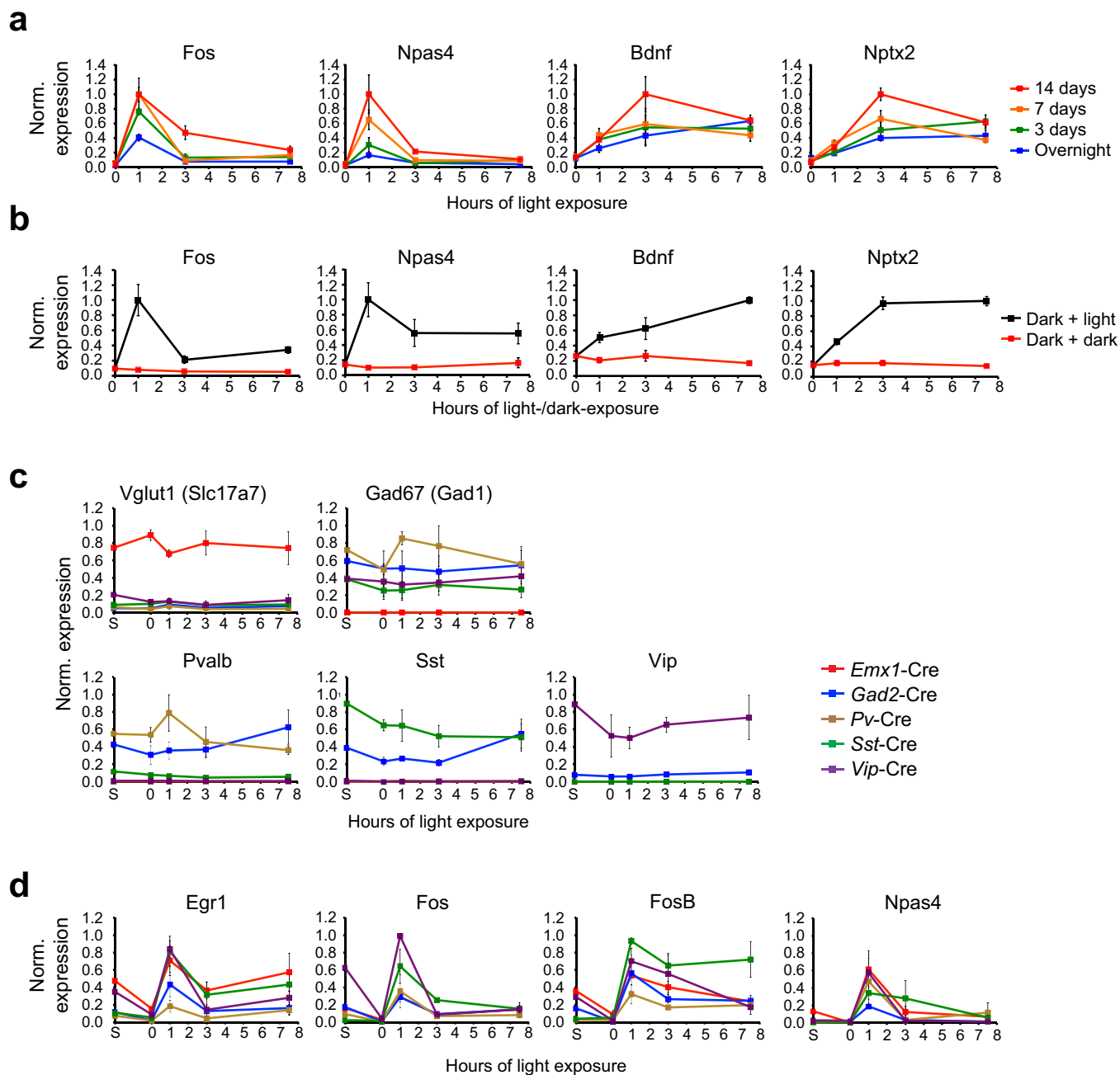
Mouse visual-evoked potential (VEP). VEPs were recorded from anaesthetized mice (50 mg kg⁻¹ Nembutal and 0.12 mg chlorprothixene) using standard techniques described previously³². The contra- and the ipsilateral eye of the mouse were presented with horizontal black and white sinusoidal bars that alternated contrast (100%) at 2 Hz. A tungsten electrode was inserted into the binocular visual cortex at 2.8 mm from the midline where the visual receptive field was approximately 20° from the vertical meridian. VEPs were recorded by filtering the signal from 0.1–100 Hz and amplifying 10,000 times. VEPs were measured at the cortical depth where the largest amplitude signal was obtained in response to a 0.05 c.p.d. stimulus (400–600 μm); 3–4 repetitions of 20 trials each were averaged in synchrony with the abrupt contrast reversal. The signal was baseline corrected to the mean voltage of the first 50 ms post-stimulus-onset. VEP amplitude was calculated by finding the minimum voltage (negative peak) within a 50–150 ms post-stimulus-onset time window. Acuity was calculated only from the deprived eye. For each different spatial frequency, 3–4 repetitions of 20 trials each were averaged in synchrony with the abrupt contrast reversal. VEP amplitude was plotted against the log of

the different spatial frequency, and the threshold of visual acuity was determined by linear extrapolation to 0 μV.

Animal husbandry and colony management. *Igf1* conditional knockout mice¹⁵, Ai9 tdTomato reporter mice³³, *Emx1-cre*³⁴, *Pv-cre*³⁵, *Gad2-cre*, *Sst-cre*, *Vip-cre*³⁶ and RiboTag mice⁸ are available from The Jackson Laboratory.

For routine experimentation, animals were genotyped using a PCR-based strategy; PCR primer sequences are available at the The Jackson Laboratory's website. For RiboTag experiments, mice homozygous for the RiboTag allele were crossed to mice homozygous for the *cre* allele and all experiments were performed with mice double heterozygous for both the RiboTag and the *cre* alleles. For *Igf1* cKO experiments, mice heterozygous for the *Igf1* conditional allele (*Igf1*^{fl/wT}) and homozygous for the *Vip-cre* allele were crossed to mice heterozygous for the *Igf1* conditional allele and homozygous for the tdTomato reporter allele. Resulting littermates all had one copy of the *Vip-cre* transgene and the tdTomato Cre reporter and yielded *Igf1*^{wT/wT} and *Igf1*^{fl/fl} littermates for experimentation. For injections of AAV constructs in the visual cortices of Cre mice (*Vip*-, *Pv*-, *Sst*-, or *Emx1-cre*), mice homozygous for the *cre* allele were crossed to wild-type C57Bl6 mice and offspring heterozygous for the *cre* allele were used for experiments. The use of animals was approved by the Animal Care and Use Committee of Harvard Medical School and/or the University of California Berkeley.

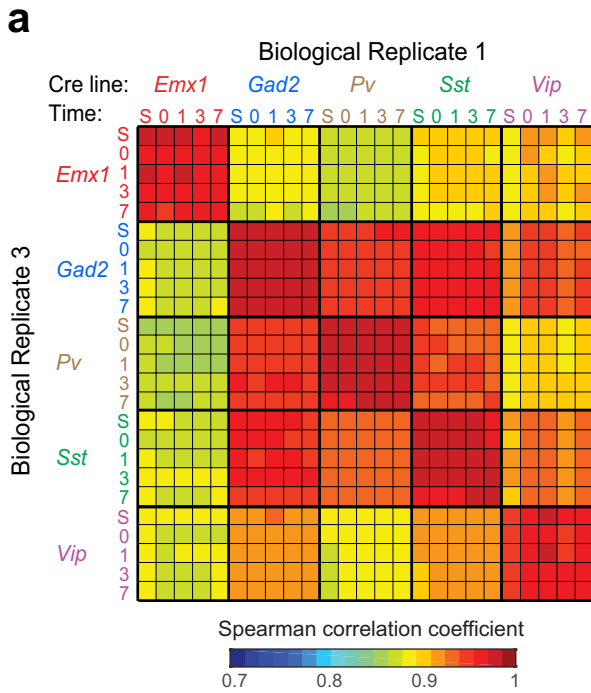
24. Livak, K. J. & Schmittgen, T. D. Analysis of relative gene expression data using real-time quantitative PCR and the 2^{-ΔΔC_T} method. *Methods* **25**, 402–408 (2001).
25. Trapnell, C. *et al.* Differential gene and transcript expression analysis of RNA-seq experiments with TopHat and Cufflinks. *Nature Protocols* **7**, 562–578 (2012).
26. Rubinson, D. A. *et al.* A lentivirus-based system to functionally silence genes in primary mammalian cells, stem cells and transgenic mice by RNA interference. *Nature Genet.* **33**, 401–406 (2003).
27. Schopman, N. C. T., Liu, Y. P., Konstantinova, P., ter Brake, O. & Berkhout, B. Optimization of shRNA inhibitors by variation of the terminal loop sequence. *Antiviral Res.* **86**, 204–211 (2010).
28. Spiegel, I. *et al.* A central role for Necl4 (SynCAM4) in Schwann cell-axon interaction and myelination. *Nature Neurosci.* **10**, 861–869 (2007).
29. Schaeren-Wiemers, N. & Gerfin-Moser, A. A single protocol to detect transcripts of various types and expression levels in neural tissue and cultured cells: in situ hybridization using digoxigenin-labelled cRNA probes. *Histochemistry* **100**, 431–440 (1993).
30. Tiscornia, G., Singer, O. & Verma, I. M. Production and purification of lentiviral vectors. *Nature Protocols* **1**, 241–245 (2006).
31. Gordon, J. A. & Stryker, M. P. Experience-dependent plasticity of binocular responses in the primary visual cortex of the mouse. *J. Neurosci.* **16**, 3274–3286 (1996).
32. Durand, S. *et al.* NMDA receptor regulation prevents regression of visual cortical function in the absence of Mecp2. *Neuron* **76**, 1078–1090 (2012).
33. Madisen, L. *et al.* A robust and high-throughput Cre reporting and characterization system for the whole mouse brain. *Nature Neurosci.* **13**, 133–140 (2010).
34. Gorski, J. A. *et al.* Cortical excitatory neurons and glia, but not GABAergic neurons, are produced in the *Emx1*-expressing lineage. *J. Neurosci.* **22**, 6309–6314 (2002).
35. Hippenmeyer, S. *et al.* A developmental switch in the response of DRG neurons to ETS transcription factor signaling. *PLoS Biol.* **3**, e159 (2005).
36. Taniguchi, H. *et al.* A resource of Cre driver lines for genetic targeting of GABAergic neurons in cerebral cortex. *Neuron* **71**, 995–1013 (2011).



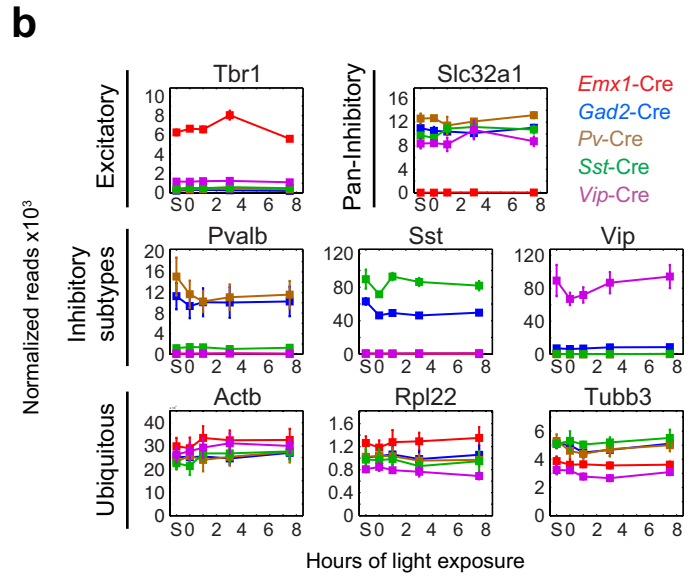
Extended Data Figure 1 | Validation of the sensory stimulation protocol and the RiboTag-based cell-type-specific purification of mRNA.

a. Quantitative real-time PCR (qPCR) for known experience-regulated genes on RNA isolated from the visual cortex of mice that were dark-housed for varying durations (overnight, 3 days, 7 days or 14 days) and then either euthanized in the dark or exposed to light for 1, 3 or 7.5 h, and then euthanized. Data are normalized to the maximal value in each data set and represent the mean and standard error of four biological replicates. **b.** qPCR for known experience-regulated genes on RNA isolated from the visual cortex of mice that were dark-housed for 14 days and then either exposed to light for 1, 3 or 7.5 h (dark + light, black) or kept in the dark

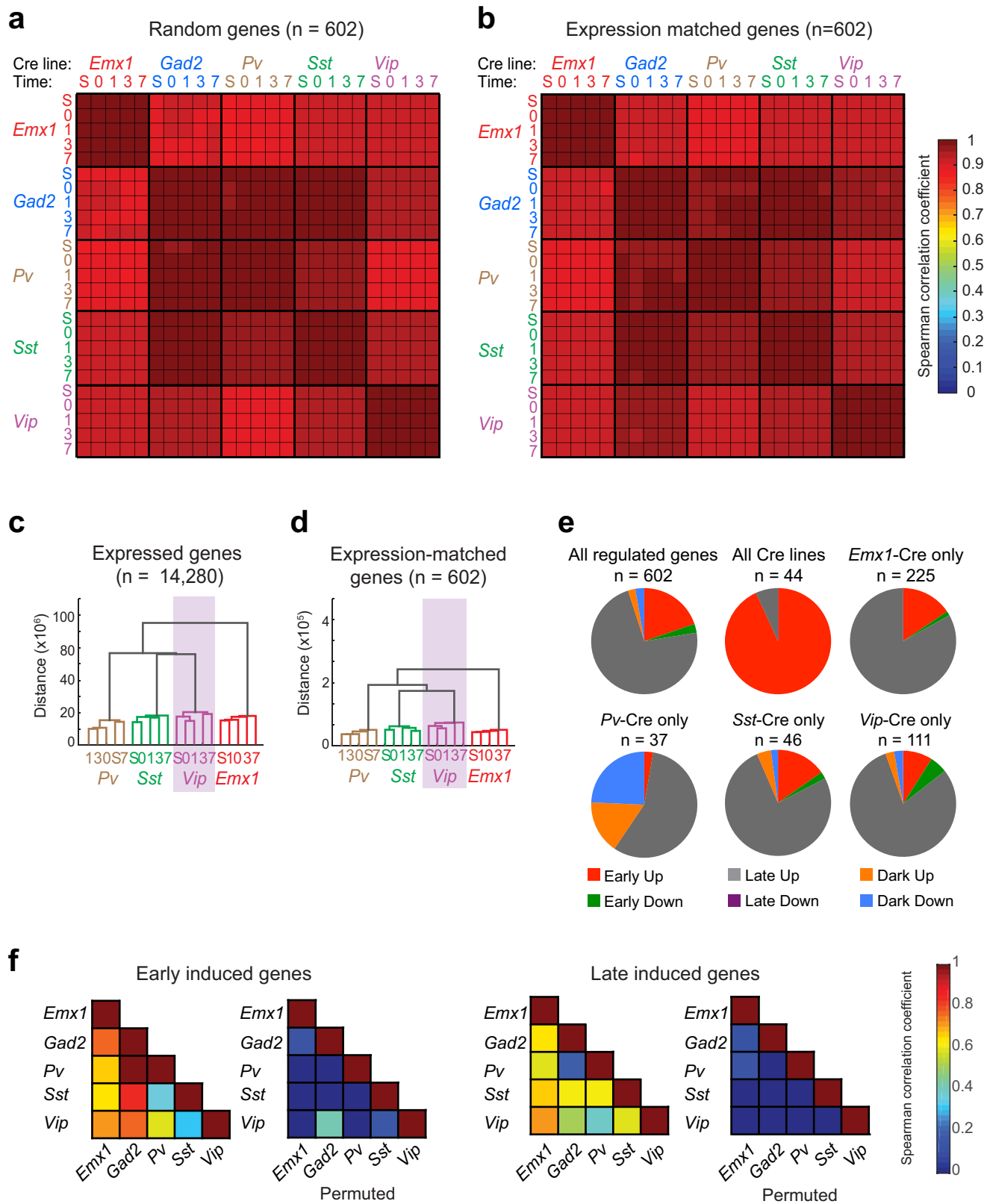
during these hours (dark + dark, red). All mice of a given time point were dissected in very close temporal proximity. Data are normalized to the maximal value in each data set and represent the mean and standard error of four biological replicates. **c.** qPCR for known cell-type-specific marker genes on RNA isolated from RiboTag mice expressing Cre in distinct neuronal subtypes. Data are normalized to the maximal value in each data set and represent the mean and standard error of three biological replicates. **d.** qPCR for known early-induced transcription factors on RNA isolated from RiboTag mice expressing Cre in distinct neuronal subtypes. Data are normalized to the maximal value in each data set and represent the mean and standard error of three biological replicates.



Extended Data Figure 2 | Validation of the RiboTag-seq approach.
a, Matrix of Spearman correlation coefficients between biological replicates across all samples (scale of correlation coefficients extends from 0.7 to 1, see colour bar) (S, standard housing; 0, dark-housed only; 1/3/7.5, 1/3/7.5 h of light exposure after dark housing, respectively). **b**, Line plots of RNA-seq data showing the expression values (normalized reads across



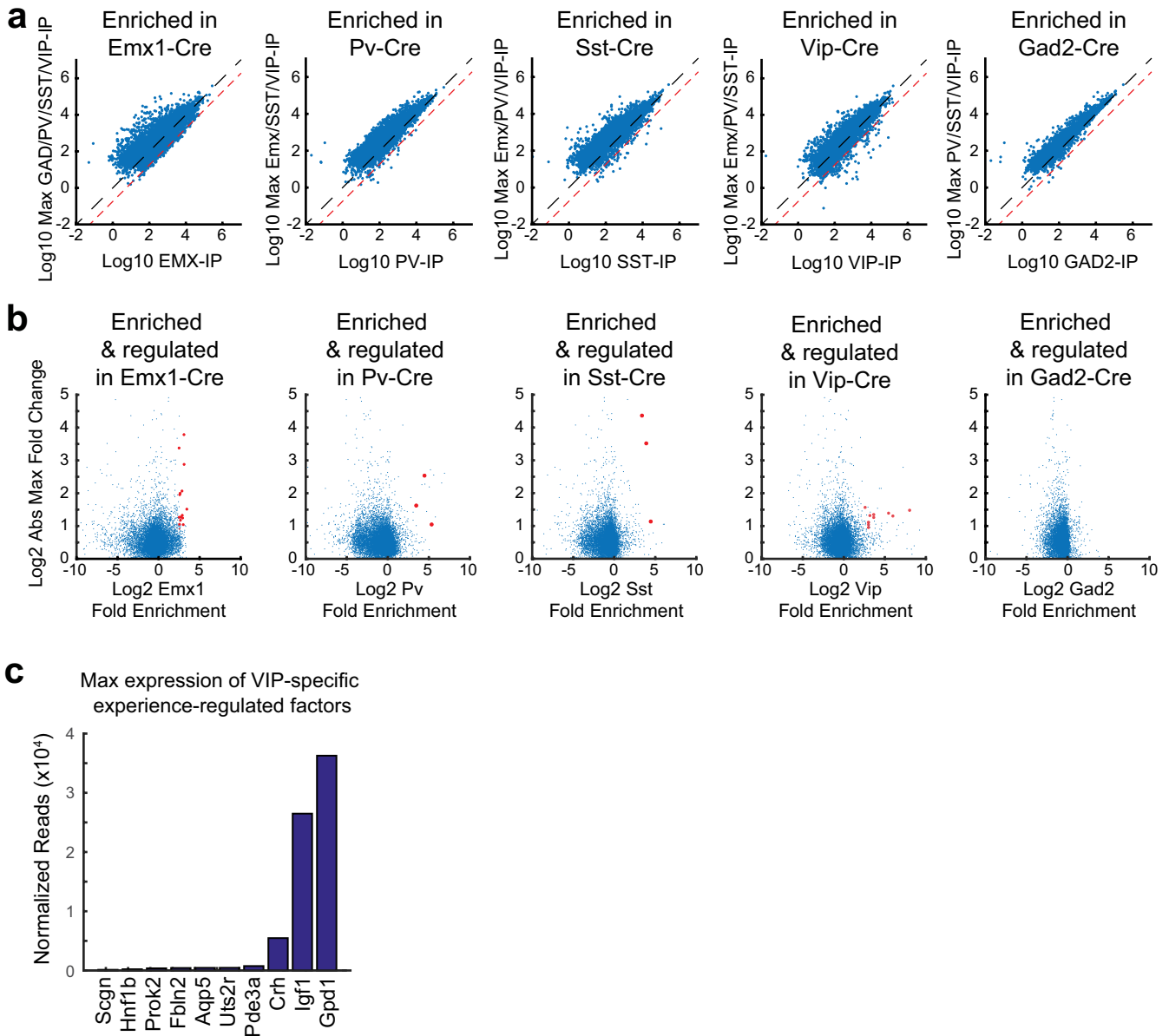
all exons of a gene) for cell-type-specific marker genes and ubiquitously expressed house-keeping genes in different Cre lines (*Emx1-cre*, red; *Gad2-cre*, blue; *Pv-cre*, brown; *Sst-cre*, green; *Vip-cre*, purple) across all time points of the experiment. Data represent the mean and standard error of three biological replicates.



Extended Data Figure 3 | See next page for caption.

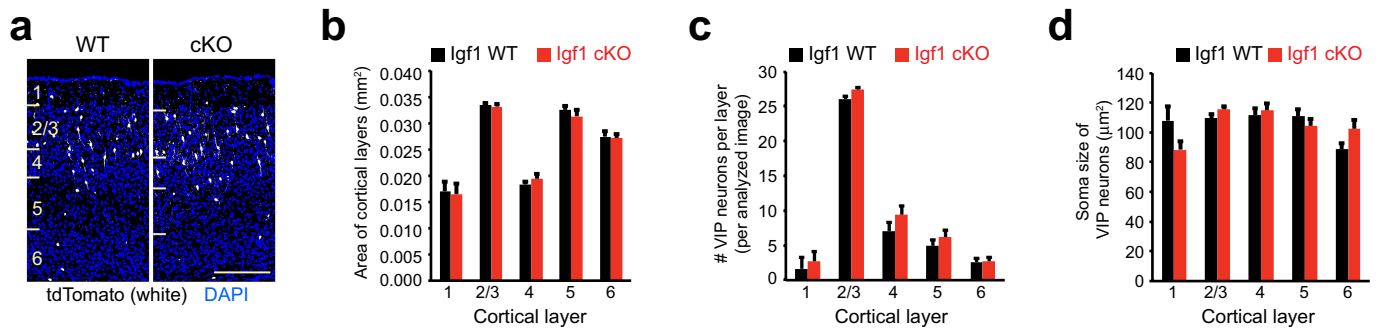
Extended Data Figure 3 | Characterization of the experience-induced gene programs in subtypes of cortical neurons. **a**, Average matrix of Spearman correlation coefficients computed from the expression values of 1000 random sets of 602 genes (including experience-regulated genes, with replacement). **b**, Matrix of the Spearman correlation coefficients computed from the expression levels of control transcripts that match the expression distribution of experience-regulated genes ($n = 602$). **c**, Cladogram resulting from hierarchical clustering of all samples (except samples from *Gad2-cre*). Cladograms were computed using the mean expression values (that is, normalized reads across all exons of a gene) for all expressed transcripts ($n = 14,280$). **d**, Cladogram resulting from hierarchical clustering of the mean expression values of a set of control transcripts that match the expression distribution of experience-regulated genes ($n = 602$).

e, Pie charts showing the subdivision of experience-regulated genes on the basis of kinetics in each set of Cre lines (red, rapidly induced; grey, induced with delayed kinetics; orange, induced only after two weeks of dark housing; green, rapidly suppressed; magenta, suppressed with delayed kinetics; blue, suppressed only after two weeks of dark housing). **f**, Left, matrix of Spearman correlation coefficients between Cre lines computed using the mean expression values (normalized reads across all exons of a gene) of early-induced genes one hour after light exposure. Right, matrix of Spearman correlation coefficients between Cre lines computed using the mean expression values of late-induced genes 7.5 h after light exposure. For each matrix, the correlations upon permuting the expression values are also shown (colour scale at right, scale begins at zero.)



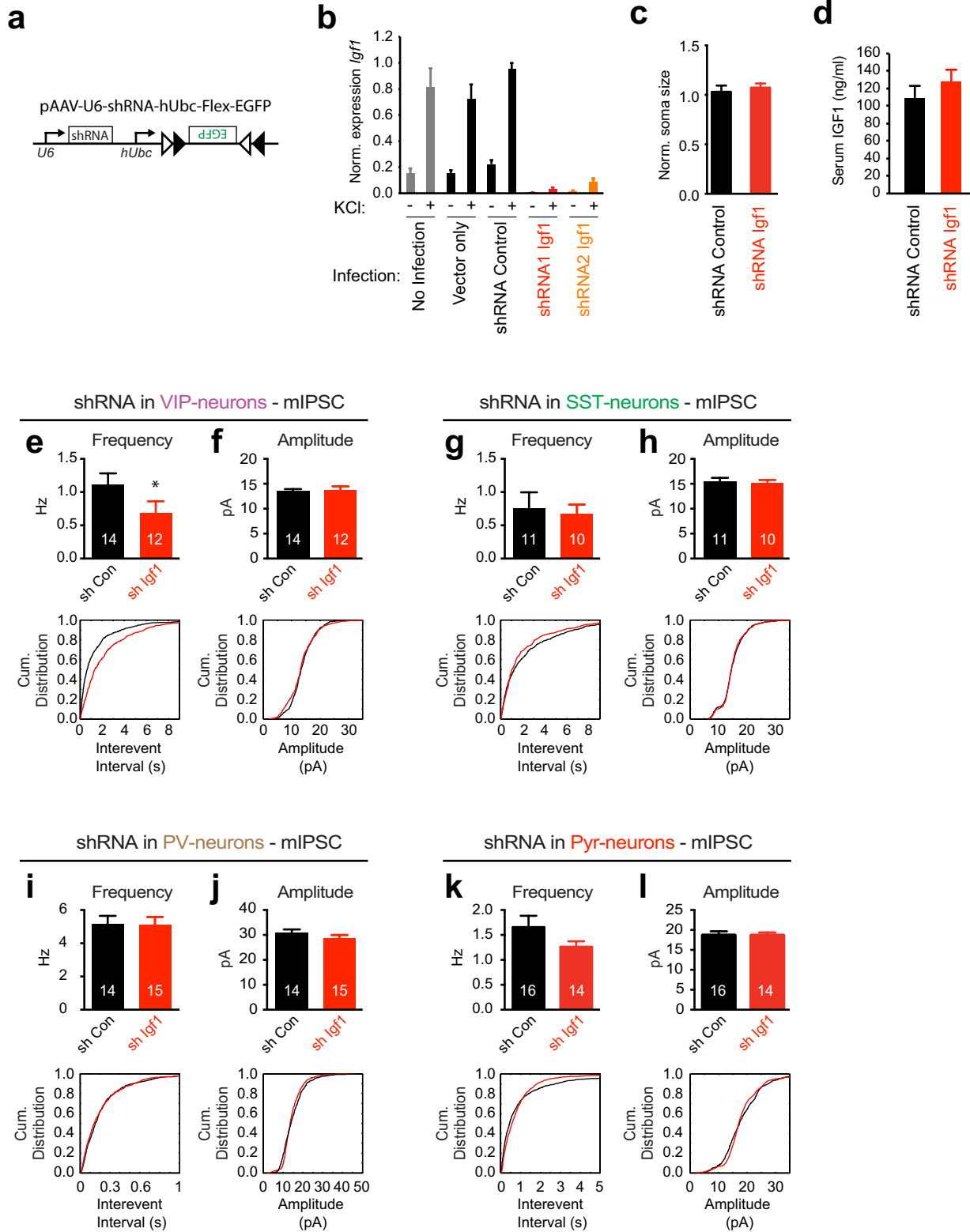
Extended Data Figure 4 | Characterization of cell-type-specific and experience-induced genes in subtypes of cortical neurons. **a**, Scatter plots showing the \log_{10} expression values for each expressed gene in a given Cre line (x axis) plotted against the maximum \log_{10} expression values for that gene found in all other Cre lines (y axis). Black line denotes unity, and the red line is the 5.5-fold enrichment threshold set to include *Vglut1* as a cell-type-specific gene in *Emx1-cre*. Data represent the mean values of three biological replicates. **b**, Scatter plots of all expressed genes,

for each Cre line plotting the mean \log_2 fold enrichment in that Cre line (x axis) against the mean \log_2 of the absolute value of the maximum fold change observed in that Cre line. Data represent the mean values of three biological replicates. Genes that pass both enrichment and induction thresholds in 3 of 3 biological replicates are shown in red. **c**, Bar graph showing the maximum expression value (in normalized reads) for VIP-neuron-specific experience-regulated genes.



Extended Data Figure 5 | Conditional knockout of *Igf1* in VIP neurons does not affect cortical morphology or gross morphology of VIP neurons. **a**, Example image of cortices from *Igf1* wild-type (WT) (*Vip-crel*⁺, *LSL-tdTomato*⁺, *Igf1*^{WT/WT}) or conditional-knockout (cKO) (*Vip-crel*⁺, *LSL-tdTomato*⁺, *Igf1*^{fl/fl}) mice. VIP neurons are labelled in

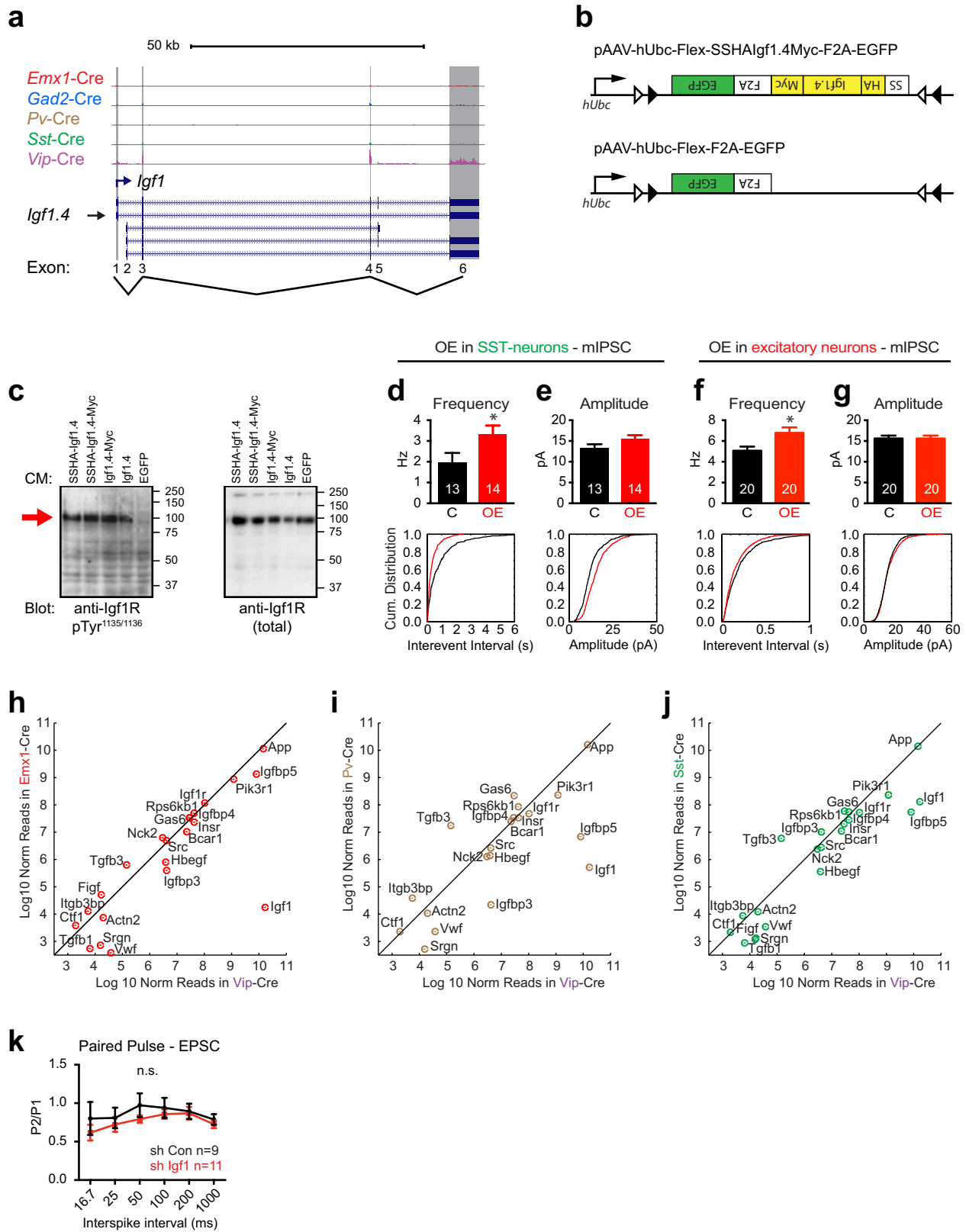
white, with DAPI shown in blue (cortical layers are indicated on the left, scale bar, 200 µm). **b–d**, Bar graphs showing the area of each cortical layer (**b**), number of VIP neurons per image per layer (**c**), or soma size of VIP neurons (**d**) in *Igf1* wild-type (black) or conditional-knockout (red) mice. Data represent the mean and standard error of three biological replicates.



Extended Data Figure 6 | See next page for caption.

Extended Data Figure 6 | *Igf1* knockdown in VIP neurons affects inhibitory inputs onto VIP neurons but not onto neighbouring neurons. **a**, AAV shRNA constructs. shRNA cassettes against *Igf1* or a control gene (*Luc*) were cloned downstream of the U6 promoter into an AAV vector that drives Cre-dependent expression of eGFP. **b**, qPCR validation of the efficacy of *Igf1* shRNA constructs. Cultured cortical neurons were infected with lentiviral constructs either expressing no shRNA (vector only), a control shRNA (against *Luc*) or shRNAs against *Igf1*. Four days post-infection the cultures were quieted overnight with TTX and AP-5 and then harvested either before or after being depolarized with 55 mM KCl for 6 h; RNA was then isolated and qPCR was performed. Data are normalized to the maximal value in each replicate and represent the mean and standard error of three biological replicates. **c**, Bar graph showing normalized soma size of P21 visual cortex VIP neurons infected with control shRNA or shRNA targeting *Igf1* (shRNA control, $n = 103$; shRNA *Igf1*, $n = 174$; $P = 0.41$, Mann–Whitney *U*-test). **d**, Bar graphs

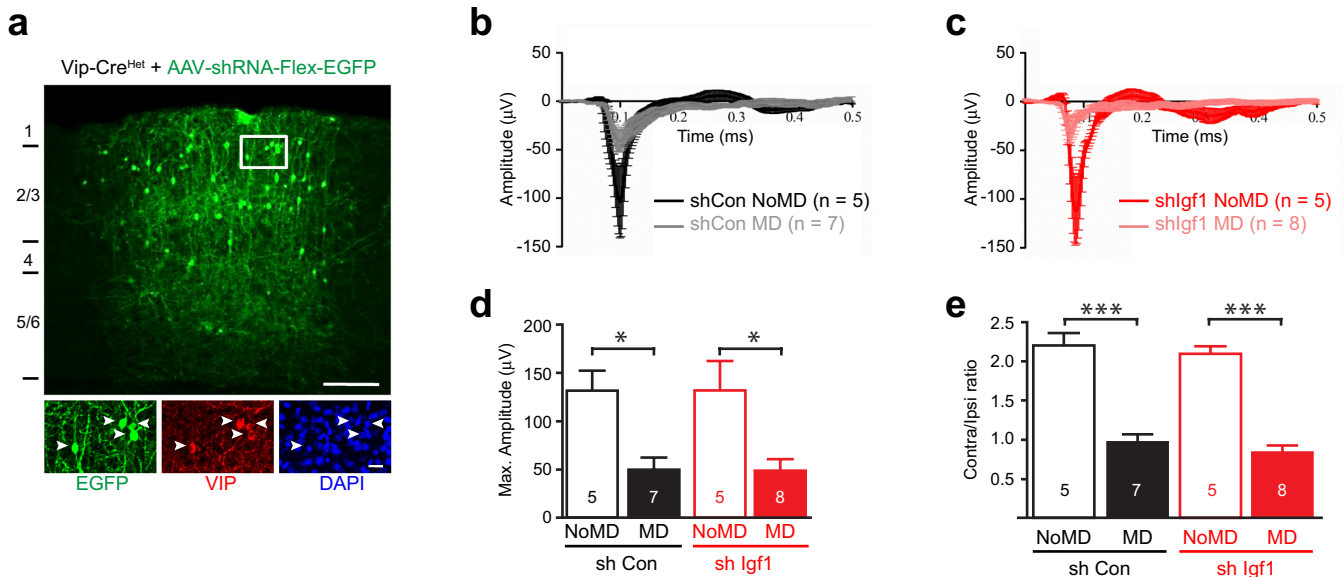
showing the levels of IGF1 in the serum of P20 mice that were injected intracortically with AAVs driving the expression of control shRNA (black) or *Igf1* shRNA. Data represent the mean and s.e.m. of the serum IGF1 levels of four mice per group. **e–l**, Bar graphs and cumulative distribution plots showing mIPSC amplitudes and frequency/inter-event interval upon early widespread knockdown of *Igf1* in VIP (**e, f**), SST (**g, h**), PV (**i, j**) and excitatory (**k, l**) neurons after injection of AAVs into P3 cortices of the respective Cre mice. VIP neurons (identified as eGFP-positive cells in *Vip-cre* mice): control and *Igf1* shRNA, amplitude $P = 0.96$, frequency $P = 0.04$. SST neurons (identified as eGFP-positive cells in *Sst-cre* mice): control and *Igf1* shRNA, amplitude $P = 0.89$, frequency $P = 0.55$. PV neurons (identified as eGFP-positive cells in *Pv-cre* mice): control and *Igf1* shRNA, amplitude $P = 0.084$, frequency $P = 0.93$. Pyramidal neurons (identified by morphology): control and *Igf1* shRNA, amplitude $P = 0.84$, frequency $P = 0.15$). All *P* values are derived from Mann–Whitney *U*-tests; numbers inside bars indicate the number of cells recorded.



Extended Data Figure 7 | See next page for caption.

Extended Data Figure 7 | Effects of IGF1 overexpression in excitatory and SST-positive neurons. **a**, RiboTag-seq identifies *Igf1.4* as the major *Igf1* isoform expressed in VIP neurons. Representative tracks of histograms of the RNA-seq reads in each Cre line across the *Igf1* genomic locus. Data are from the 7.5 h light exposure RiboTag-seq data sets. **b**, AAV constructs for the Cre-dependent expression of HA-/Myc-tagged IGF1 (*Igf1.4*) and eGFP (that is, IGF1-OE, top) or of eGFP alone (that is, control, bottom). F2A, Furin cleavage site followed by the 2A peptide; black and white triangles represent a Cre-dependent Flex-switch. **c**, Western blot analysis of IGF1-receptor activation status in lysates of serum starved HEK293T cells that were stimulated with conditioned media (CM) containing epitope-tagged isoforms of IGF1. CM was produced by transfecting HEK293T cells with the respective construct and collecting the culture media. IGF1-receptor is detected with antibodies against either activated IGF1 receptor (anti-IGF1R pTyr^{1136/1138}) or total IGF1 receptor (anti-IGF1R total). Molecular weight markers are on the right and the arrow indicates the band of the IGF1 receptor. **d, e**, Bar graphs and cumulative distribution plots showing mIPSC frequency/

inter-event interval (**d**) and amplitude (**e**) of mIPSCs recorded from eGFP-positive neurons in P20 *Sst-cre* mice that were intracortically injected with AAVs driving the expression of control (C) or IGF1-OE (OE) constructs (amplitude, $P = 0.16$; frequency, $P = 0.01$; Mann-Whitney U -test; numbers inside bars indicate the number of cells recorded). **f, g**, Bar graphs and cumulative distribution plots showing mIPSC frequency/inter-event interval (**f**) and amplitude (**g**) of mIPSCs recorded from eGFP-positive neurons in P20 *Emx1-cre* mice that were intracortically injected with AAVs driving the expression of control (black, $n = 20$) or IGF1-OE AAVs (red, $n = 20$). Amplitude, $P = 0.99$; frequency, $P = 0.01$, Mann-Whitney U -test. **h-j**, Scatter plots of IGF1-interacting proteins showing the \log_{10} normalized mean expression values in *Vip-cre* neurons versus each of the other Cre lines (*Emx1* (**h**), *Pv* (**i**), *Sst* (**j**)). **k**, Quantification of EPSC paired-pulse recordings from VIP neurons infected with control shRNA- (black $n = 9$) or *Igf1* shRNA- (red $n = 11$) expressing AAVs. The ratio of the second EPSC amplitude divided by the first EPSC amplitude is plotted against inter-stimulus interval ($P = 0.1$, two-way ANOVA).



Extended Data Figure 8 | VIP neuron-derived IGF1 does not disrupt ocular dominance plasticity. **a**, Widespread infection of VIP neurons by AAV-shRNA-hUbc-Flex-eGFP. High-titre injection of AAVs into the visual cortex of P18–20 *Vip-cre*⁺ mice leads to infection of the majority VIP neurons (green, eGFP; red, anti-VIP; blue, DAPI; arrowheads, infected VIP neurons; scale bars, 150 μ m, 20 μ m in the inset). **b**, **c**, Average of VEP traces recorded in the visual cortices of mice that were injected with AAVs expressing control shRNA (black/grey) or shRNA against *Igf1* (red/pink) shRNA and that were (grey, pink) or were not (black, red) subjected to monocular deprivation in the eye contralateral to the recording site (MD versus NoMD, respectively). **d**, Monocular deprivation

induces a significant reduction in the VEP amplitude in response to low spatial frequency stimulation in mice that had AAVs expressing control shRNA and *Igf1* shRNA injected into their visual cortices (control shRNA NoMD, $n = 5$ mice; control shRNA MD, $n = 7$ mice; *Igf1* shRNA NoMD, $n = 5$; *Igf1* shRNA MD, $n = 8$). * $P < 0.05$, Mann–Whitney *U*-test). **e**, Mice that had AAVs expressing control shRNA (black) and *Igf1* shRNA (red) injected into their visual cortices display normal ocular dominance plasticity as monocular deprivation (MD) induces a shift to the ipsilateral eye in both groups (control shRNA NoMD, $n = 5$ mice; control shRNA MD, $n = 7$; *Igf1* shRNA NoMD, $n = 5$; *Igf1* shRNA MD, $n = 8$ mice. *** $P < 0.0001$, one-way ANOVA with Tukey's post hoc test).